JOURNAL OF AGRICULTURAL AND FOOD CHEMISTRY

pubs.acs.org/JAFC Article

Odorant-Binding Protein Interactions with Herbivore-Induced Volatiles Drive Behavioral Attraction of *Harmonia axyridis* (Coleoptera: Coccinellidae) to Tuta Absoluta-Infested Tomato Plant

Tijjani Mustapha,[⊥] Youdan Zhang,[⊥] Jianquan Yan, Huatao Tang, Zhujun Wang, Sheng-Yen Wu, Abdul Basit, Yassir Boulaamane, Anshuman Chandra, Mai-Abba Ishiyaku Abdullahi, Moazam Hyder, and Youming Hou*

Cite This: https://doi.org/10.1021/acs.jafc.6c01340 Read Online

ACCESS | Metrics & More | Article Recommendations | Supporting Information

ABSTRACT: *Tuta absoluta* severely constrains global tomato production. We investigated the behavioral attraction of *Harmonia axyridis* to infested plants and the molecular basis of herbivore-induced plant volatile (HIPV) recognition. Y-tube bioassays showed statistically significant attraction of *H. axyridis* to the infested plant (χ^2 = 13.72, P < 0.05). Molecular docking showed strong HaxyOBP-HIPV interactions, with predicted binding energies reaching −7.6 kl mol^{-1} and ligand efficiencies of more than 0.30 kl mol^{-1} per heavy atom. HaxyOBP13, HaxyOBP19, and HaxyOBP23 were found to have the most stable complexes with 1,3-cyclohexadiene-1-carboxaldehyde, 2,6,6-trimethyl, 1-methyl-3-(1-methylethyl), and beta-phellandrene during 100 ns molecular dynamics simulations, maintaining RMSD values within 0.15−0.30 nm. The competitive binding assays confirmed micromolar affinities, with dissociation constants (K_d) ranging between 6.45 and 14.58 μM. These behavioral, computational, and biochemical findings define important OBPs that mediate the perception of HIPV in *H. axyridis*, which forms the basis of volatile-mediated improvement of biological control measures against *T. absoluta*.

KEYWORDS: *Harmonia axyridis, Tuta absoluta, tomato, herbivore-induced plant volatiles (HIPVs), odorant-binding proteins (OBPs), biological control*

INTRODUCTION

The tomato leafminer, *Tuta absoluta*, causes significant yield losses for the widely grown tomato (*Solanum lycopersicum*). Known as "the Ebola virus of tomato", this devastating pest threatens the global tomato crop by causing yield losses in uncontrolled or poorly managed environments in South America, the Mediterranean, Africa, and Asia that can range from 40% to 100%.[1,2] Because of the high reproductive potential of *T. absoluta* of up to 12 generations seasonally and its hidden larval stages that feed within plant tissues, the species has developed a rapid resistance to a wide range of chemical insecticides, making management challenges significant in reducing these losses.[3] Chemical techniques have grown less effective; thus, biological control strategies have evolved as very effective and long-term alternatives. These include the employment of predatory insects such as ladybirds and the mirid bug *Nesidiocoris tenuis*, which are important biocontrol agents capable of reducing fruit infestations by up to 100% once established.[4] The most successful IPM strategies incorporate these biological agents. For example, the synergistic use of Bt and *N. tenuis* has been found to dramatically boost marketable yields and minimize fruit damage by 90−93%,[3] giving a long-term option to mitigate the severe economic impact of *T. absoluta*.[5,6]

Herbivore-induced plant volatiles (HIPVs) play a critical role in plant defense and tritrophic signaling by attracting the natural enemies of herbivores, such as ladybird beetles. These volatiles are released by plants like tomatoes when they are attacked by herbivores such as *T. absoluta*,[7] serving as chemical signals that guide beneficial predators to locate their prey. For example, HIPVs released by aphid-infested plants contribute to the attraction of ladybird beetles, standing as the major natural predators of aphids, thereby enhancing the resistance of the affected plant to the herbivorous attacks.[1,2] Furthermore, olfactory recognition of HIPVs depends on odorant-binding proteins (OBPs) found in beneficial predators such as ladybird beetles (*H. axyridis*). At the molecular level, OBPs play a key role in the initial recognition and transport of volatile compounds within the insect olfactory system. These olfactory system proteins bind to and transport HIPVs as an odorant molecule to odorant receptor on the surface of receptors via the sensillum lymph. Therefore, the ability of the predator, particularly *H. axyridis*, to detect and respond to these volatile cues is facilitated by this binding, which in turn enhances their ability to forage and prey on herbivores.[3,8]

Recent studies in predatory insects have begun to uncover the molecular basis of HIPV perception, highlighting the role

Received: January 24, 2026
Revised: March 17, 2026
Accepted: March 18, 2026

of odorant-binding proteins (OBPs) as key mediators of volatile recognition. For example, in the mirid predator *Macrolophus pygmaeus*, specific OBPs have been shown to bind herbivore-induced tomato volatiles with high affinity and selectivity, and functional analyses indicate that only a subset of the OBP repertoire contributes directly to prey- or host-associated odor detection. These findings suggest that the apparent redundancy of OBP gene families in predatory insects reflects functional specialization toward chemically diverse HIPVs rather than nonspecific binding capacity. However, despite the ecological importance and widespread use of the ladybird *Harmonia axyridis* in biological control programs, the molecular mechanisms underlying its perception of HIPVs remain largely unexplored. In particular, it is unknown how its expanded OBP repertoire contributes to the recognition of volatiles emitted by herbivore-infested plants. Guided by insights from OBP−HIPV interactions in other predatory insects, we hypothesized that HIPV recognition in *H. axyridis* is mediated by a limited subset of functionally specialized OBPs. This rationale motivated the systematic screening of 31 HaxyOBPs using integrated computational and experimental approaches to prioritize candidate proteins involved in HIPV detection.

While it is known that HIPVs mediate an interaction between plants, herbivores, and natural enemies,[9] the precise molecular mechanism governing the olfactory behavior of predators like *H. axyridis* remains an ongoing area of research. The complexity of HIPV blends and the specific appeal of generalist predators are two major drawbacks. For instance, adults of *H. axyridis* are attracted to both the volatiles of the insectary plant *Cnidium monnieri* and *Vitex negundo* infected with *Aphis gossypii*.[9,10] The generalist predator, *M. pygmaeus*, can also distinguish *T. absoluta*-infested plants when compared with noninfested tomato plants using HIPVs.[11] Nevertheless, the detailed profile of HIPVs of *T. absoluta*-infested tomato plants that mediate *H. axyridis* orientation is not clearly identified. Previous studies have reported the release of distinct volatile compounds from tomato plants attacked by *T. absoluta* or *Bemisia tabaci*,[7,12] influencing the behavior of some natural enemies such as *N. tenuis* and *Macrolophus basicornis*.[12,13] Nevertheless, the picture of which particular HIPV compound *H. axyridis* perceives and how such perceptions are converted into behavioral responses is still at an early stage.

Another limitation is the "black box" nature of olfactory perception at the molecular level. While OBPs are known to be the first step in recognizing volatiles, transporting odors through sensillum lymph to odorant receptors (ORs),[14,15] the precise binding interactions between specific HIPVs and OBPs in *H. axyridis* have not been fully mapped. *H. axyridis* has a sensitive olfactory system in *H. axyridis* is highly specialized for locating its prey,[15] and 19 OBPs have been identified in its antennae,[14] while another study identified 31 OBPs,[16] with four antennae-enriched OBPs characterized for binding affinity.[15] Despite the successful identification and characterization, their specific binding affinities to the complex array of HIPVs emitted by *T. absoluta*-infested tomato plants are not yet fully understood. This lack of specific data limits the ability to predict and manipulate the response of *H. axyridis* to infested plants effectively.

Studying the interactions between HIPVs and OBPs using molecular docking and dynamic simulation techniques can enhance the understanding of these interactions and improve the biological control of *T. absoluta* with the help of *H. axyridis*. Therefore, computationally screening a library of known HIPVs from *T. absoluta*-infested tomato plants against the identified OBPs of *H. axyridis* can identify the most promising HIPV-OBP pairs with high binding affinities.[14,15,17] Based on prior evidence that herbivore-induced plant volatiles mediate predator attraction and that odorant-binding proteins play a central role in volatile recognition, we formulated the following hypotheses: (i) *T. absoluta*-infested tomato plants emit specific HIPVs that elicit behavioral attraction in *H. axyridis*; (ii) these HIPVs bind with high affinity and specificity to a subset of *H. axyridis* odorant-binding proteins, rather than uniformly across the OBP repertoire; and (iii) terpenoid and aldehyde HIPVs, which dominate the volatile profile of infested plants, exhibit particularly stable interactions with functionally specialized HaxyOBPs. To test these hypotheses, we combined behavioral assays, computational docking and molecular dynamics simulations, ligand efficiency analysis, and experimental fluorescence binding assays to identify and validate key OBP−HIPV interactions underlying predator attraction.

MATERIALS AND METHODS

Insect Culture and Infestation

Eggs of the multicolored Asian ladybird beetle (*H. axyridis*) were obtained from Keyun Biological Resources (Henan Jiyuan Baiyun Industry Co., Ltd., China) and hatched to produce a colony. These colonies were reared on an aphid (*Acyrthosiphon pisum*) supply on a potted Egyptian broad bean under controlled environmental conditions (25 ± 2 °C 65 ± 5% RH, 16:8D photoperiod). All beetles used in behavioral assays were maintained on the same aphid species for at least one generation prior to experimentation to ensure uniform olfactory experience. Importantly, beetles had no prior exposure to tomato plants or *T. absoluta* before the olfactometer assays. Adult beetles aged 5−10 days postemergence were used in bioassays. Similarly, tomato plants (*S. lycopersicum*) were grown in 2 L pots in a controlled temperature, relative humidity and light condition (25 ± 2 °C, 65 ± 5% RH, 16:8D photoperiod), where plants at the 5−8 leaf stage were used in the experiment. For infestation, 20 s-third instar larvae of *T. absoluta* were carefully placed on each plant and allowed to feed for 48 h prior to bioassay. The control plants were handled but remained uninfested. Adult *H. axyridis* of mixed sex were used in all Y-tube olfactometer bioassays. Individuals were randomly selected and used only once, and the sex ratio was approximately balanced across treatments.

Y-Tube Olfactometer Bioassay

Behavioral assays were conducted using a glass Y-tube olfactometer (main arm: 10 cm; side arms: 8 cm each; internal diameter: 3 cm) positioned at an angle of 60 °C.[10] Briefly, charcoal-filtered and humidified air was pushed through each arm at a flow rate of 300 mL min^{-1} using an air delivery system. One arm was connected to a glass chamber (2 L) containing a *T. absoluta*-infested tomato plant, while the other contained a healthy plant. To avoid directional bias, the position of the odor sources was alternated between replicates. Subsequently, individual beetles were released at the base of the main arm and allowed 5 min to make a choice, defined as crossing 3 cm into one of the side arms, consistent with previous olfactory studies on beetle predators,[18] where responsive individuals typically make a directional choice within the first few minutes of exposure. Preliminary observations indicated that beetles failing to respond within this time frame rarely made consistent choices thereafter. Therefore, the 5 min window was considered sufficient to capture active olfactory responses while minimizing random movement or fatigue effects. Beetles not making a choice were recorded as "no response". After each replicate, the Y-tube olfactometer was thoroughly cleaned with 70% ethanol, rinsed with distilled water, and oven-dried at 65 °C before the next assay. In addition, odor

https://doi.org/10.1021/acs.jafc.6c01340
J. Agric. Food Chem. XXXX, XXX, XXX−XXX

delivery lines were flushed with clean air between trials to minimize residual volatile contamination. Thus, the Y-tube olfactometer bioassay was conducted in six independent experimental replicates. In each replicate, 30 naïve adult *H. axyridis* individuals were individually released into the olfactometer and each beetle was tested only once and was not reused in any subsequent replicate or treatment. Therefore, a total of 180 independent beetles were evaluated per treatment. Individual beetles were treated as independent biological units for statistical analysis, while replicates represented independent experimental runs conducted on different occasions.

Ligand Preparation

Twenty-three HIPVs (Table S1) differentially released by tomato during *T. absoluta* infestation were curated from a previous study based on their association with tomato defense as proven by volatilome analyses.[7] The chemical information on these volatiles was retrieved from PubChem (https://pubchem.ncbi.nlm.nih.gov/) on 25th May, 2025, where the PubChem ID and 3D Structure Data File (SDF) of each individual compound were obtained. For HIPVs without available 3D structure, their SMILES notations were converted into 3D structures, energy-minimized and converted into Protein Data Bank Partial Charge and Atom Type (pdbqt) files using Open Babel within Python Prescription (PyRx) virtual screening tool.[19]

Protein Homology Modeling

A total of 31 antennal OBP sequences from *H. axyridis* were obtained from a previous study as fully characterized by Rondoni et al.[16] Their tertiary structures were modeled using AlphaFold2 (DeepMind Technologies Ltd., London, UK).[20] The modeled structures were validated using standard stereochemical parameters. For further model quality assessment, DeepUMQA-X (Institute of Computing Technology, Chinese Academy of Sciences, Beijing, China) server was used to evaluate the local residue accuracy (lDDT) and overall folding accuracy (TM-score) of the predicted protein structures (Table S2).[21] The stereochemical quality of all predicted OBP structures was further evaluated using Ramachandran plot analysis (Figures S1A,B) generated with BIOVIA Discovery Studio, 2025 Client (Dassault Systèmes). To reduce the computational cost and improve the accuracy of predictions, Computed Atlas of Surface Topography of the Universe of protein Folds (CASTpFold) was used to determine the binding pocket of each OBP prior to the initiation of the docking process, where the area ($Å^2$) and volume ($Å^3$) of each binding pocket were recorded, respectively (Table S3).[22]

Phylogenetic Analysis

The amino acid sequences of 31 HaxyOBP proteins were aligned with MAFFT v7 using the automatic strategy. The resulting alignment comprised 360 amino acid sites across 31 sequences. The alignment was subjected to maximum-likelihood (ML) phylogenetic inference using IQ-TREE v2.2.6 (COVID edition, Dec 2023 build).[23] ModelFinder was employed to determine the best-fit model of sequence evolution according to the Bayesian Information Criterion (BIC).[24] The WAG + F + I + G4 model (Whelan and Goldman empirical substitution matrix with empirical amino acid frequencies, proportion of invariant sites, and gamma-distributed rate heterogeneity with four categories) was selected as optimal. Branch support was assessed with 1000 ultrafast bootstrap replicates (UFBoot) combined with SH-aLRT branch tests to provide robust support estimation.[25] Patristic (tree-based) pairwise evolutionary distances were calculated from the resulting ML tree and visualized as a symmetric heatmap to assess relative sequence divergence among OBPs. The ML tree was visualized in a circular layout with bootstrap support values mapped to branch colors. Functional annotations (binding free energy, ligand efficiency, and molecular dynamics stability) were subsequently overlaid on the phylogeny to relate evolutionary divergence to predicted ligand-binding properties.

Molecular Docking. Molecular docking simulations were performed using AutoDock Vina (The Scripps Research Institute, La Jolla, CA, USA) within the PyRx interface. Protein models of the 31 HaxyOBPs were inspected in PyMOL Molecular Graphics System Version 3.1.6.1 (Schrödinger, LLC, New York, NY, USA), protonated for pH 7.0, and prepared as PDBQT files after adding polar hydrogens and Gasteiger charges. To account for receptor flexibility, an ensemble docking strategy was employed. Three representative OBP binding-pocket conformations were extracted from stable regions of the molecular dynamics trajectories based on RMSD clustering analysis. These conformations were subsequently used as independent receptors for docking to capture pocket flexibility effects, and each was prepared as a receptor in PDBQT, and 24 HIPVs ligands were docked individually.[26] The docking grid was centered on pocket centroids and sized to encompass the pocket. Default PyRx Vina parameters were used for this docking workflow, and the best ligand-OBP binding affinities (ΔG) in kcal mol^{-1} were extracted and tabulated.

Ligand Efficiency (LE) Analysis

Ligand efficiency (LE) was computed to normalize binding affinities by ligand size and to enable the ranking of HIPV-OBP complexes in an atom-economical manner.[27] This approach allows direct comparison of binding efficiencies among ligands of different molecular sizes. The LE was calculated as the absolute value of the binding free energy divided by the number of heavy atoms in the ligand, performed using in-house scripts implemented in R Studio v4.5.1 (R Foundation for Statistical Computing, Vienna, Austria). Binding energies (ΔG, kcal mol^{-1}) obtained from the docking result were combined with ligand heavy atom counts (N_{HA}) derived from SMILES structures using Open Babel, Version 2.4.1 (Graphical User Interface), Open Babel Development Team (http://openbabel.org). Thus, the calculation was used according to the formula

$$LE = \frac{|\Delta G|}{N_{HA}}$$

where $|\Delta G|$ is the best predicted absolute binding affinity for a given ligand-OBP pair and N_{HA} is the number of non-hydrogen atoms.

All docking outputs were collected in to a master results table in R Studio (V4.5). The workflow parsed Vina log files to extract ΔG values, merged these with ligand atom counts, and computed LE automatically. Complexes were ranked first by ΔG and subsequently by LE, allowing the identification of ligands with strong binding affinities that also show favorable atom efficiency. Top-ranking complexes were selected for downstream interaction profiling. Visualizations of LE distributions across ligands and OBPS was performed in R Studio using violin plots and heatmaps, facilitating the detection of consistent high-efficiency ligands.

Interaction Pattern Analysis

Top complexes were analyzed using molecular interaction profiling tool (Discovery Studio Visualizer 2025 client) to examine hydrogen bonds, $\pi-\pi$ stacking, van der Waals interactions, and hydrophobic contacts within the binding pockets. Both 2- and 3-dimensional interaction models were retrieved and compiled accordingly.

Molecular Dynamics Simulation (MDS)

Six OBP-ligand complexes, selected based on their highest docking scores, were prepared for molecular dynamics (MD) simulations. The complexes were processed using the Protein Preparation Wizard in Maestro 12.5 to correct structural defects.[28] Missing side chains and loops were modeled using Prime. MD simulations were performed in Desmond (Schrödinger LLC, New York, NY, USA) to investigate structural changes within a solvated environment.[29] The solvated system was constructed using the System Builder, with the complex centered in an orthorhombic box under periodic boundary conditions. The box was filled with Single Point Charge (SPC) water molecules, ensuring a minimum distance of 10 Å between any protein atom and the box boundaries. The system was neutralized by the addition of sodium and chloride ions, and isotonic conditions were established by supplementing with 0.15 M NaCl. Energy minimization and relaxation of the system were carried out using the OPLS3e force field.[30] The production simulations were conducted under constant

https://doi.org/10.1021/acs.jafc.6c01340
J. Agric. Food Chem. XXXX, XXX, XXX−XXX

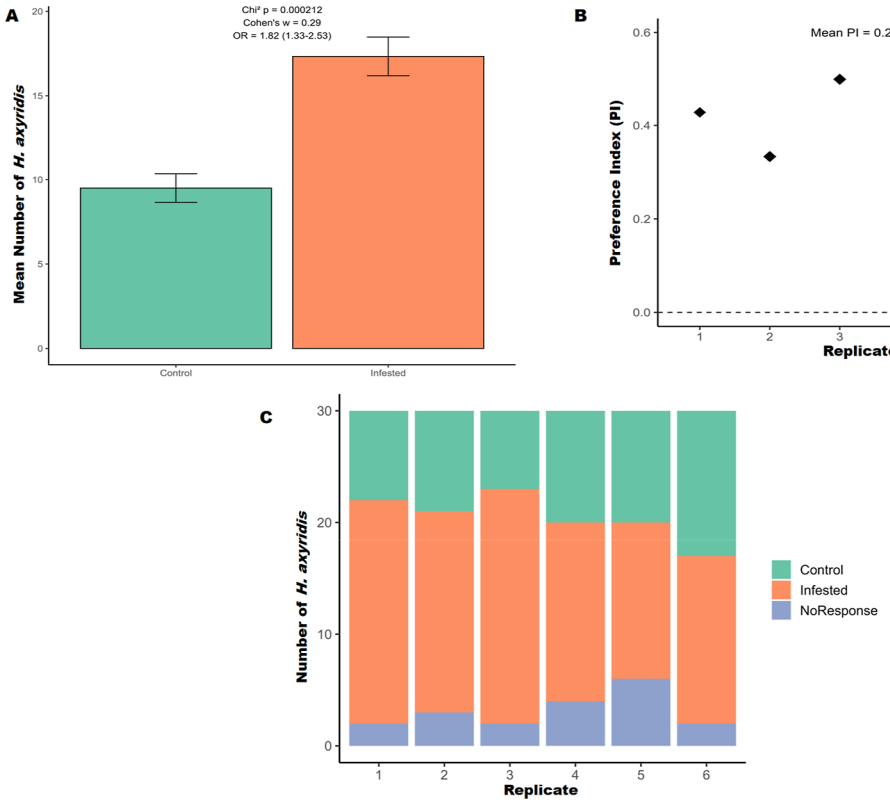

Figure 1. Beetle preference for infested plants. (A) Mean number of beetles (±SE) on control and infested plants. Beetle distribution differed significantly between treatments (χ^2 = 13.72, p = 0.0002; OR = 1.82, 95% CI: 1.33−2.53). (B) Preference index (PI) across six replicates (mean PI = 0.29 ± 0.07 SE), consistently positive toward infested plants. (C) Stacked bar plots of beetle responses per replicate, showing most beetles aggregated on infested plants, with fewer on controls and a minor fraction showing no response.

temperature (300 K) and pressure (1 atm), regulated by the Nose−Hoover thermostat and the Martyna−Tobias−Klein barostat, respectively.[31] Each simulation was run for a total of 100 ns, with 1000 trajectory frames recorded for subsequent analysis. Trajectories were evaluated using the simulation interaction diagram (SID) tool to examine structural stability, conformational fluctuations, and protein−ligand interactions throughout the course of the simulation.

For the transitions to experimental validation, HaxyOBP13, HaxyOBP19, and HaxyOBP23 were selected for recombinant expression and fluorescence binding assays based on multicriteria prioritization. These OBPs consistently ranked among the top candidates according to (i) lowest docking binding energies with major HIPVs, (ii) favorable ligand efficiency values, and (iii) structural stability during 100 ns molecular dynamics simulations. All three proteins exhibited stable RMSD trajectories and maintained conserved hydrophobic binding cavities throughout simulations, indicating structurally reliable ligand accommodation. This integrative computational filtering guided experimental validation.

Expression and Purification of Recombinant HaxyOBPs

The open reading frame (ORF) sequences of *H. axyridis* odorant-binding proteins HaxyOBP13, HaxyOBP19, and HaxyOBP23, excluding their predicted signal peptides, were codon-optimized for *E. coli* expression and synthesized according to a previous study (Li et al., 2024). Each gene was cloned into the pET-28b expression vector, which provides an N-terminal 6xHis-tag followed by a thrombin cleavage site. The recombinant plasmids were transformed into *E. coli* BL21(DE3) competent cells for protein expression. A single positive colony for each OBP was used to inoculate a starter culture in Lysogeny Broth (LB) medium containing 50 μg/mL kanamycin, grown overnight at 37 °C with shaking at 220 rpm. This starter culture was diluted 1:100 into fresh LB-kanamycin medium. The cells were grown at 37 °C until the optical density at 600 nm (OD_{600}) reached approximately 0.6. Protein expression was induced by adding isopropyl β-D-1-thiogalactopyranoside (IPTG) to a final concentration of 0.5 mM, and the culture was incubated for an additional 20 h at 18 °C with shaking. Cells were harvested by centrifugation at 8000*g* for 10 min at 4 °C. The cell pellet was resuspended in lysis buffer (50 mM Tris−HCl, 300 mM NaCl, 10 mM imidazole, pH 8.0) supplemented with 1 mg/mL lysozyme and a protease inhibitor cocktail. The cells were lysed by sonication on ice, and the cell debris was removed by centrifugation at 15,000*g* for 30 min at 4 °C. However, the recombinant His-tagged proteins were purified using Ni-Nitrilotriacetic acid (Ni-NTA) agarose resin (Qiagen) according to the manufacturer's instructions. Briefly, the supernatant was incubated with pre-equilibrated resin for 1 h at 4 °C. The resin was washed extensively with wash buffer (50 mM Tris−HCl, 300 mM NaCl, 30 mM imidazole, pH 8.0) to remove nonspecifically bound proteins. The target proteins were eluted with elution buffer (50 mM Tris−HCl, 300 mM NaCl, 300 mM imidazole, pH 8.0). The 6xHis-tag was removed by incubating the eluted protein with thrombin (1 U/mg protein) overnight at 4 °C. The cleaved tag and thrombin were removed by a second pass over the Ni-NTA resin. The purity and molecular weight of the final proteins were verified by 15% sodium dodecyl sulfate-polyacrylamide gel electrophoresis (SDS-PAGE). Purified proteins were dialyzed extensively against 50 mM Tris−HCl buffer (pH 7.4), concentrated using a centrifugal filter unit (Amicon, 10 kDa MWCO), aliquoted, and stored at −80 °C. Protein concentration was determined using the Bradford assay with bovine serum albumin (BSA) as a standard.

Fluorescence Competitive Binding Assays

The binding affinities of the purified HaxyOBPs for selected volatile organic compounds (VOCs) were determined using a fluorescence competitive binding assay with *N*-phenyl-1-naphthylamine (1-NPN) as the fluorescent probe. All measurements were performed on an F-4600 fluorescence spectrophotometer (Hitachi) at 25 °C using a 1 cm path length quartz cuvette (Li et al., 2024). First, the binding affinity

https://doi.org/10.1021/acs.jafc.6c01340
J. Agric. Food Chem. XXXX, XXX, XXX−XXX

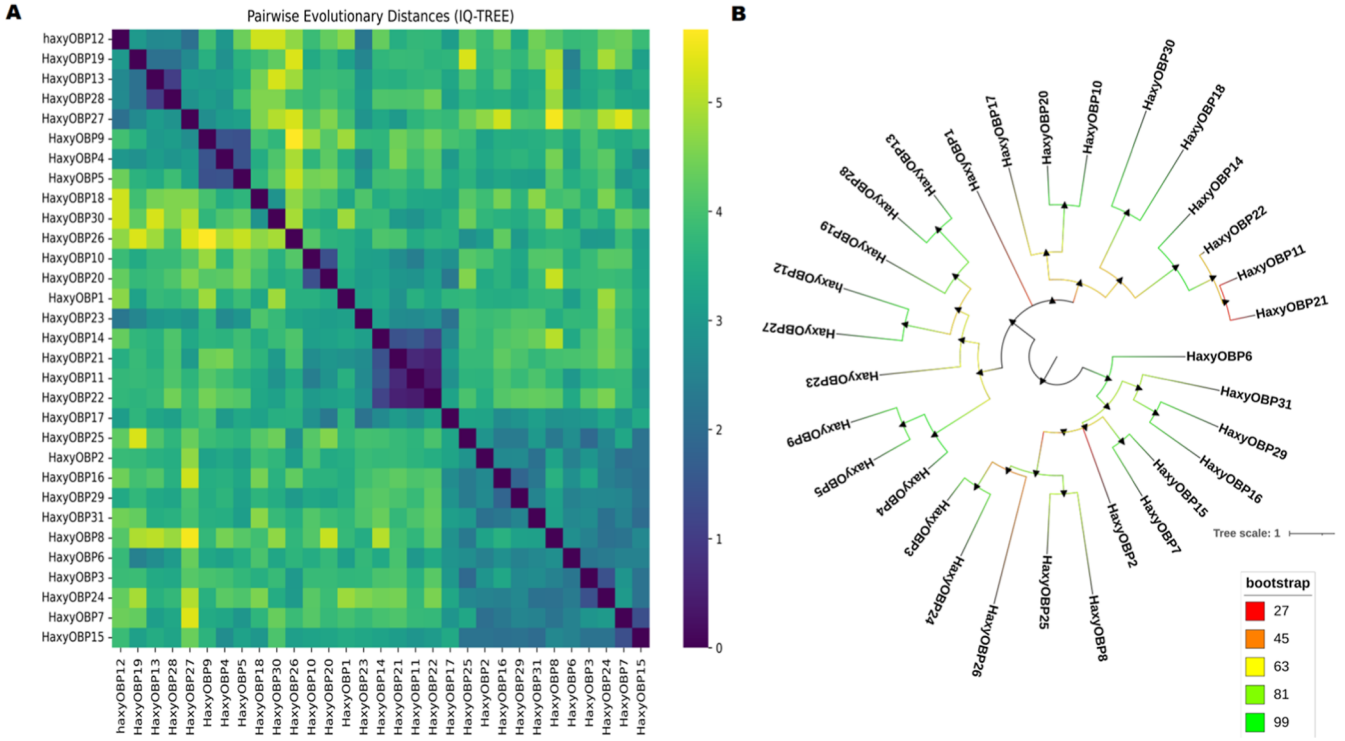

Figure 2. Phylogenetic relationships and pairwise evolutionary distances among 31 *HaxyOBP* sequences. (A) Pairwise evolutionary-distance heatmap derived from the maximum-likelihood alignment: darker squares indicate lower evolutionary distance (closer sequences). Distances are patristic (tree-based) pairwise distances computed from the ML tree and visualized as a symmetric heatmap (scale at right). (B) Maximum-likelihood phylogeny inferred with IQ-TREE. Branch colors indicate bootstrap.

of 1-NPN for each OBP was characterized. A 2 μM solution of protein in 50 mM Tris−HCl buffer (pH 7.4) was titrated with aliquots of a 1 mM stock solution of 1-NPN in HPLC-grade methanol. The fluorescence intensity was measured after each addition, with an excitation wavelength of 337 nm and an emission scan from 350 to 500 nm. The dissociation constant (K_d) of the probe for each protein was calculated from the saturation curve using the Scatchard equation. For competitive binding assays, a solution containing 2 μM OBP and 2 μM 1-NPN (at the K_d concentration) was prepared. This protein-probe complex was then competitively titrated with each candidate ligand. The three VOCs tested were 1,3-cyclohexadiene-1-carboxaldehyde and 2,6,6-trimethyl (Safranal) for HaxyOBP13; benzene, 1-methyl-3-(1-methylethyl)- (*m*-Cymene) for HaxyOBP19; and β-phellandrene for HaxyOBP23. A 1 mM stock solution of each ligand in HPLC-grade methanol was used for titration. The fluorescence intensity at the emission maximum was recorded after each ligand addition. The affinity of the competitor ligand is expressed as the inhibition constant (K_i), which was calculated from the measured half-maximal inhibitory concentration (IC_{50}) using the Cheng-Prusoff equation

$$K_i = \frac{IC_{50}}{1 + \frac{[1 - NPN]}{KD(1 - NPN)}}$$

where [1−NPN] is the free concentration of the fluorescent probe and $K_{D(1-NPN)}$ is its dissociation constant for the protein. Each assay was performed in triplicate, and one-way ANOVA was used to determine significant differences, with statistical significance defined by a *p*-value less than 0.05.

Statistical Analysis

Beetle choice data were analyzed using a chi-square goodness-of-fit test to determine whether the distribution between control and infested plants deviated from random expectation. Effect size was quantified using Cohen's *w*, providing an estimate of the magnitude of treatment effects. To further evaluate the strength of association, odds ratios (OR) with 95% confidence intervals were calculated, comparing the likelihood of *H. axyridis* selecting infested versus control plants. For a quantitative measurement of the relative attraction of *H. axyridis* to *T. absoluta*-infested tomato plants versus control plants in the Y-tube olfactometer assay, a preference index (PI) was also computed for each replicate, with mean values and associated standard errors reported to capture variation in preference strength across trials. The preference index was calculated using the following formula

$$PI = \frac{N_{infested} - N_{control}}{N_{control} + N_{control}}$$

where $N_{infested}$ and $N_{control}$ represent the number of insects choosing the infested and control odor sources, respectively. The PI ranges from −1 to +1, with positive values indicating preference for infested plants, negative values indicating preference for control plants, and values close to zero indicating no preference. All statistical analyses were performed using R Studio v4.5.1 (R Foundation for Statistical Computing, Vienna, Austria).

RESULTS

Behavioral Response (Choice Test)

In Y-tube olfactometer assays, ladybird beetles displayed a clear preference for volatiles emitted by *T. absoluta*-infested tomato plants compared to uninfested controls (Figure 1). There were notable differences in the distribution of *H. axyridis* between the infested and control plants (Figure 1A). Strong deviation from random choice was shown by a chi-square test (χ^2 = 13.72, p = 0.0002, Table S4). A Cohen's w of 0.29, which is consistent with a medium biological effect, was obtained from effect size estimation. Additionally, odds ratio analysis revealed that, with a 95% confidence interval of 1.33−2.53, beetles were 1.82 times more likely to be found on infested plants than controls. The PI, which averaged 0.29 ± 0.07 (SE) over six

https://doi.org/10.1021/acs.jafc.6c01340
J. Agric. Food Chem. XXXX, XXX, XXX−XXX

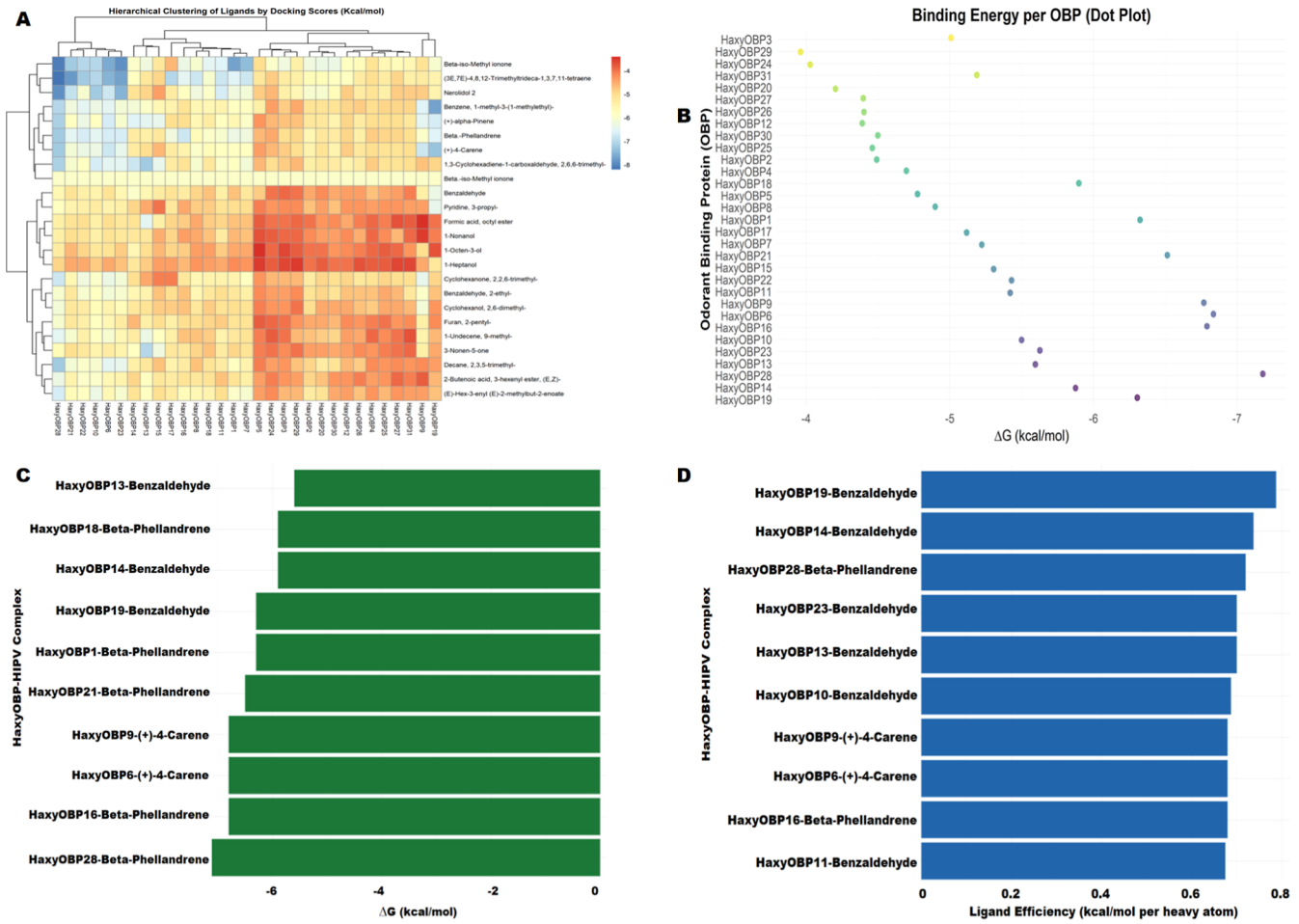

Figure 3. Integrated analysis of OBP−HIPV binding affinities and ligand efficiency. (A) Heatmap showing docking-derived binding free energies (kcal·mol^{-1}) for all herbivore-induced plant volatile (HIPV)−odorant-binding protein (OBP) pairs. (B) Dot plot illustrating the overall distribution of binding energies across all OBP−HIPV interactions. (C) Ranking of the top OBP−HIPV complexes based on binding free energy (kcal·mol^{-1}). (D) Ranking of top OBP−HIPV complexes based on ligand efficiency (LE; kcal·mol^{-1} per heavy atom), highlighting ligands with high binding efficiency relative to molecular size.

replicates, was used to measure preference variation at the replicate level (Figure 1B). PI values consistently showed a bias toward infested plants, despite the strength of individual replicates varying. However, the positive PI values indicated a preference for *T. absoluta*-infested plants. Further evidence of this pattern was provided by stacked bar plots summarizing beetle counts across response categories (control, infested, and no response); most beetles clustered on infested plants, fewer selected controls, and only a small percentage did not respond (Figure 1C). These findings show that infestation greatly increases plant attractiveness to *H. axyridis*, leading to a repeatable preference for infested hosts.

HaxyOBP Phylogenetic Analysis

Phylogenetic analysis of the 31 *HaxyOBP* sequences resolved multiple distinct clades and revealed heterogeneous sequence divergence across the family (Figure 2A,B). In Figure 2A, areas with low intersequence distance represent closely related paralog groups, while lighter areas indicate greater divergence between other OBP pairs. The tree in Figure 2B shows well-defined groups with strong support (indicated by branch color), but some splits have weaker support and need careful consideration. These groupings will help understand how ligands bind and the stability dynamics seen in subsequent docking and molecular dynamics simulation (MDS) analyses.

In addition to revealing conserved sequence features, the phylogenetic clustering of HaxyOBPs showed partial correspondence with ligand-binding preferences identified through docking, molecular dynamics simulations, and fluorescence binding assays. OBPs grouped within the same clade tended to display similar affinities toward specific classes of HIPVs. For instance, OBPs clustering with HaxyOBP19 and HaxyOBP13 preferentially interacted with aromatic aldehydes and related benzenoid compounds, whereas OBPs clustering with HaxyOBP23 showed stronger binding toward terpenoid compounds such as *β*-phellandrene. This pattern suggests functional convergence within certain OBP clades and indicates a degree of functional redundancy in recognizing chemically related HIPVs.

HaxyOBPs-HIPVs Binding Energy

Predicted binding free energies (ΔG) ranged from −8.2 to −3.4 kcal mol^{-1} across 23 HIPVs and 31 modeled *H. axyridis* OBPs. The complete set of docking energies for all OBP−HIPV combinations, as well as binding pocket volume descriptors for all modeled OBPs, are provided in Tables S3 and S5, respectively. The result showed that most OBP−HIPV pairs had moderate docking scores (ΔG = −5 to −6 kcal mol^{-1}), while a subset of ligand−OBP pairs showed much stronger binding (Figure 3A). A number of OBPs showed

https://doi.org/10.1021/acs.jafc.6c01340
J. Agric. Food Chem. XXXX, XXX, XXX−XXX

exceptionally high affinity for specific HIPVs. The sesquiterpene (3*E*,7*E*)-4,8,12-trimethyltrideca-1,3,7,11-tetraene bound to HaxyOBP28 the strongest (ΔG = −8.2 kcal mol^{-1}). The cyclic ketone β-iso-methyl ionone was bound by HaxyOBP21 and HaxyOBP23 with ΔG = −7.8 and −7.9 kcal mol^{-1}, respectively. The docking of HaxyOBP1, OBP6, and OBP7 to β-isomethyl ionone was also very favorable (ΔG = −7.4 to −7.7). Nerolidol 2 binding to HaxyOBP10 (ΔG = −7.2 kcal mol^{-1}), a trimethylcyclohexadiene carboxaldehyde binding to HaxyOBP13 (ΔG = −7.2) and OBP14 (ΔG = −6.8), and the C_{13} polyene binding to OBP22 (ΔG = −7.2) and OBP17 (ΔG = −7.0) are additional noteworthy high-affinity interactions. The strongest OBP−HIPV interactions found are listed in Table 1.

Table 1. Ligand Efficiency, Heavy Atoms and Binding Energy (kcal mol^{-1}) Profile of the Best Interacting HIPV-OBP Complexes OBPs Ligands (HIPV) Binding Energy Heavy Atoms LE

HaxyOBP19	benzaldehyde	−6.3	8	0.79
HaxyOBP14	benzaldehyde	−5.9	8	0.74
HaxyOBP28	Beta-phellandrene	−7.2	10	0.72
HaxyOBP13	benzaldehyde	−5.6	8	0.7
HaxyOBP23	benzaldehyde	−5.6	8	0.7
HaxyOBP10	benzaldehyde	−5.5	8	0.69
HaxyOBP16	Beta-phellandrene	−6.8	10	0.68
HaxyOBP6	(+)-4-Carene	−6.8	10	0.68
HaxyOBP9	(+)-4-Carene	−6.8	10	0.68
HaxyOBP11	benzaldehyde	−5.4	8	0.68
HaxyOBP22	benzaldehyde	−5.4	8	0.68
HaxyOBP15	benzaldehyde	−5.3	8	0.66
HaxyOBP21	Beta-phellandrene	−6.5	10	0.65
HaxyOBP7	benzaldehyde	−5.2	8	0.65
HaxyOBP17	benzaldehyde	−5.1	8	0.64
HaxyOBP1	Beta-phellandrene	−6.3	10	0.63
HaxyOBP8	benzaldehyde	−4.9	8	0.61
HaxyOBP5	benzaldehyde	−4.8	8	0.6
HaxyOBP18	Beta-phellandrene	−5.9	10	0.59
HaxyOBP4	benzaldehyde	−4.7	8	0.59
HaxyOBP2	benzaldehyde	−4.5	8	0.56
HaxyOBP25	benzaldehyde	−4.5	8	0.56
HaxyOBP30	benzaldehyde	−4.5	8	0.56
HaxyOBP12	benzaldehyde	−4.4	8	0.55
HaxyOBP26	benzaldehyde	−4.4	8	0.55
HaxyOBP27	benzaldehyde	−4.4	8	0.55
HaxyOBP20	benzaldehyde	−4.2	8	0.55
HaxyOBP31	benzaldehyde, 2-ethyl-	−5.2	10	0.52
HaxyOBP24	benzaldehyde	−4	8	0.5
HaxyOBP29	benzaldehyde	−4	8	0.5
HaxyOBP3	Beta-phellandrene	−5	10	0.5

Many OBPs were strongly bound to certain HIPVs. With 16 of the 31 OBPs, $\Delta G \leq -6.0$ kcal mol^{-1} was found for β-iso-methyl ionone, which was by far the most widely distributed (Figure 3B). Additionally, the C_{13} polyene (3*E*,7E)-4,8,12-trimethyltrideca-1,3,7,11-tetraene bonded to 13 OBPs favorably ($\Delta G \leq -6.0$). Trimethylcyclohexadiene aldehyde (10 OBPs) and β-phellandrene (both potent with 12 OBPs) were also widely effective ligands. Of the simpler monoterpenes, (+)-α-pinene and (+)-4-carene had $\Delta G \leq -6.0$ kcal mol^{-1} with 9 and 8 OBPs, respectively. These counts show which volatiles interact with the most OBPs (Figure 3A,B).

Different patterns emerged from the hierarchical clustering of the binding energy matrix (Figure 3B). Across several OBPs, a cluster of ligands consisting of hydrophobic terpenoids and ketones (β-ionone, the C_{13} tetraene, nerolidol, α-pinene, 4-carene, and β-phellandrene) produced the most negative ΔG values. Small alcohols, short-chain ketones/aldehydes, and esters were among the other ligand clusters that produced consistently weaker binding. Similarly, OBPs formed sub-clusters based on shared ligand preferences. The complete clustering heatmap is displayed in Figure 3A, and this chemical segregation is in line with the known hydrophobic binding preferences of the OBPs tested in this study.

The HIPV chemical class clearly affects the results. With their preferred OBPs, terpenoids (monoterpenes and sesquiterpenes) like α-pinene, β-phellandrene, and nerolidol tended to have the lowest ΔG values (often ≤ -6.5 kcal mol^{-1}). Similar strength was shown by cyclic ketones (ionones); for example, β-iso-methyl ionone exhibited the strongest binding across a wide range of OBPs. Aliphatic alcohols and ketones, such as heptanol, nonanol, and 3-nonen-5-one, on the other hand, bound loosely (ΔG = −5 kcal mol^{-1}). Hexenyl butenoate, methyl salicylate, and benzaldehyde are examples of small aromatics and esters that exhibited intermediate affinities (ΔG of 5 to −6), while heterocycles such as propylpyridine and pentyl furan gave the weakest binding (ΔG = 4).

In our findings, terpenoid HIPVs (particularly β-iso-methyl ionone) were the most widely active ligands, whereas OBPs 28, 23, and 21 (and related proteins) were the highest-affinity receptors (Figure 3A,B). These results show which OBPs and HIPVs are probably most important for *H. axyridis* olfaction.

Ligand Efficiency Analysis

Ligand efficiency (LE) for top-ranked OBP−HIPV complexes was calculated by normalizing binding free energy to the number of ligand heavy atoms. LE values (kcal·mol^{-1} per non-H atom) varied approximately between 0.50 and 0.79 across the data set (Figure 3A,C). Smaller HIPV ligands generally exhibit higher ligand efficiency (LE). Monoterpenes and simple aromatics (8−10 heavy atoms) bind more efficiently per atom than larger sesquiterpenes. For instance, larger terpenes (such as a 16-atom C_{17} triterpene) exhibited lower LE (∼0.5), while benzaldehyde (8 heavy atoms) consistently showed up among the highest-LE ligands. This pattern is consistent with the widespread finding that smaller ligands frequently exhibit higher LE than larger ones. The mean LE for benzaldehyde in the top-LE complexes was approximately 0.62, whereas the mean LE for β-phellandrene (10 heavy atoms) was approximately 0.63 (Table 1). A benzaldehyde−HaxyOBP complex exhibited a high ligand efficiency (LE) of approximately 0.79, confirming efficient binding of small volatiles.

Complexes of OBPs containing small aromatic and monoterpenoid volatiles had the highest LE scores (Table 1). HaxyOBP19−benzaldehyde was the only highest-LE complex (LE = 0.79, 8 heavy atoms). HaxyOBP14−benzaldehyde (LE = 0.74, 8 H atoms) and HaxyOBP28−β-phellandrene (LE = 0.72, 10 H atoms) followed closely behind. HaxyOBP13−benzaldehyde (LE = 0.70, 8 atoms) and HaxyOBP23−benzaldehyde (LE = 0.70, 8 atoms) were two other top complexes (Figure 3D). Table 1 and Figure 4A−C summarizes these top-LE complexes along with their heavy-atom counts and ΔG. The LE ranking consistently places benzaldehyde ligands (8 H atoms) at the top, suggesting that

https://doi.org/10.1021/acs.jafc.6c01340
J. Agric. Food Chem. XXXX, XXX, XXX−XXX

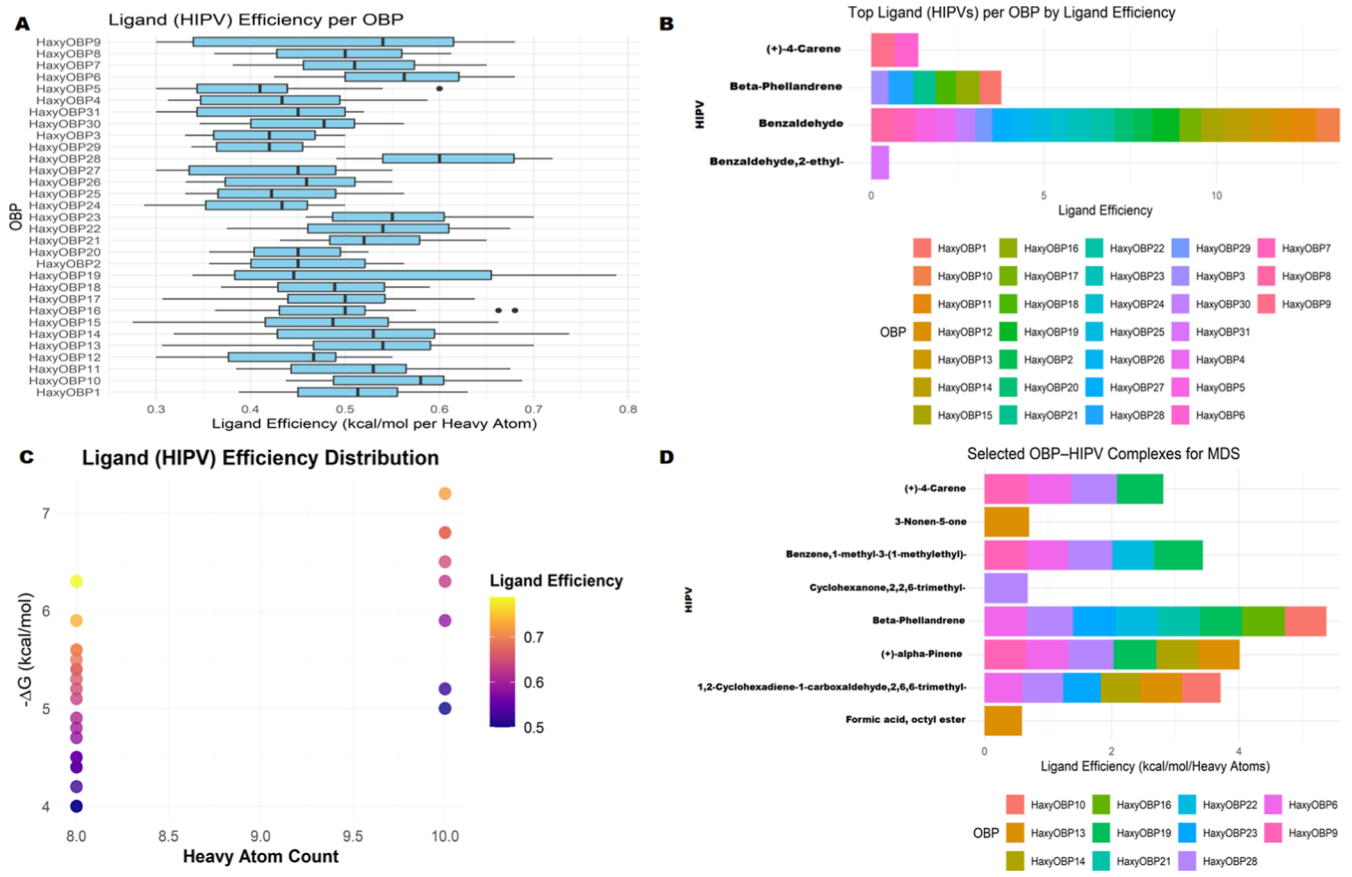

Figure 4. Ligand efficiency–based prioritization of OBP–HIPV complexes for molecular dynamics simulations. (A) Ligand efficiency (LE) values across all OBPs, expressed as binding free energy normalized by ligand heavy atom count. (B) OBP–HIPV complexes exhibiting the highest ligand efficiency, indicating favorable binding relative to ligand size. (C) Distribution of ligand efficiency as a function of binding free energy (kcal·mol^{-1}) and HIPV heavy atom number, illustrating size–affinity relationships. (D) OBP–HIPV complexes selected for molecular dynamics simulations based on combined binding energy and ligand efficiency criteria.

each non-H atom plays a significant role in binding. When bound to HaxyOBP6 and HaxyOBP9, (+)-4-carene (10 H atoms) also had a high LE (~0.68) among monoterpenes. The heavy-atom counts of these ligands are explicitly given in Table 1, highlighting that the top-LE ligands all had ≤10 non-hydrogen atoms.

Compared to ranking by binding free energy alone (Figure 5A), ranking by LE yielded a noticeably different ordering (Figure 3C). Large sesquiterpenes and triterpenes (such as long-chain isoprenoids with ΔG = −8.2 kcal mol^{-1}) were the strongest absolute binders in the prior ΔG-based analysis. These large ligands do not make the top-LE list, though, because they have a lot of heavy atoms and a lower LE (0.50–0.55). On the other hand, when normalized by size, smaller volatiles such as benzaldehyde and β-phellandrene had the highest LE (Figure 3D) despite having moderately negative ΔG (e.g., −6.3 to −7.2 kcal mol^{-1}) (see Figure 6).

Further, β-iso-methylionone and (3*E*,7*E*)-4,8,12-trimethyltridecatetraene were earlier top binders with a ΔG as low as −8.2 kcal mol^{-1} and 14–16 heavy atoms (LE = 0.50). Despite having a high ΔG ranking, these complexes rank lower than many smaller ligands in terms of LE. On the other hand, the LE list is topped by benzaldehyde–OBP complexes (ΔG ~ −5.1 to −6.3 kcal mol^{-1}). Despite having only midrange ΔG values, LE (0.7–0.8) is obtained by dividing by only 8 heavy atoms. This emphasizes how small aromatic HIPVs "punch above their weight" when it comes to binding to OBP. When efficiency is taken into account, a number of OBP–ligand pairs that were not previously ranked as the best by ΔG now show promise. For example, HaxyOBP19–benzaldehyde, LE 0.79, was not among the very top ΔG complexes but is the LE leader (Figure 4B).

These comparative findings demonstrate how LE enhances ligand prioritization by favoring ligands that bind efficiently in relation to their size, which supplements the previous energy-only ranking (Figure 4B,D). In practice, taking LE into account could aid in locating effective smaller HIPVs that binding energy alone could fail to detect.

Amino Acid Residue Interaction Analysis

According to molecular docking, several *H. axyridis* OBPs exhibited high affinities for herbivore-induced volatiles released from tomato plants infested with *T. absoluta*. The top complexes had binding free energies ranging from −6.5 to −7.7 kcal·mol^{-1} (Table 2). The result further showed that HaxyOBP19 and HaxyOBP28 consistently showed the strongest binding to monoterpenes such as (+)-4-carene and β-phellandrene (Figures 3A–D and 4B), with ΔG values as high as −7.7 kcal·mol^{-1}. Other OBPs that displayed notable affinities (−6.5 to −7.2 kcal·mol^{-1}) included HaxyOBP6. Hydrophobic and aromatic interactions were the main factors contributing to the stabilization of the OBP binding pockets, as indicated by the residue–level interaction analysis (Figures 5–7 and S2–S6).

https://doi.org/10.1021/acs.jafc.6c01340
J. Agric. Food Chem. XXXX, XXX, XXX–XXX

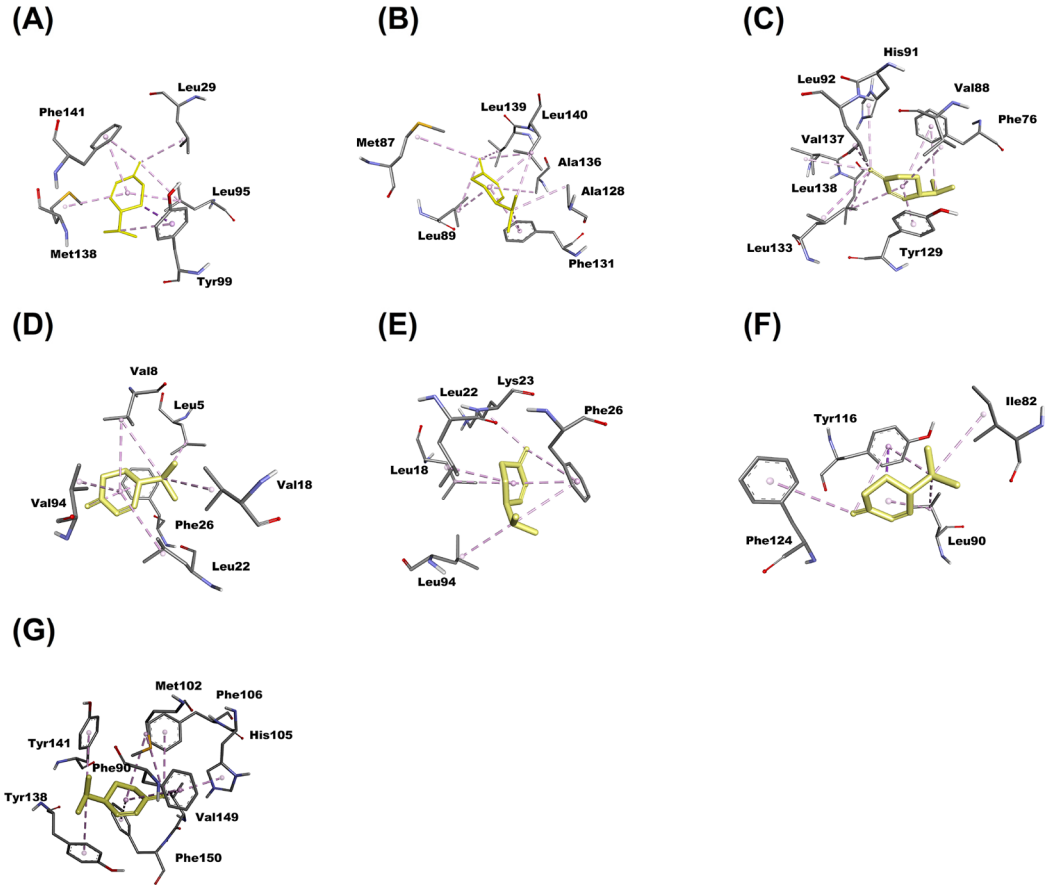

Figure 5. A 3D interaction of Beta-Phellandrene with HaxyOBP6 (A), HaxyOBP10 (B), HaxyOBP16 (C), HaxyOBP19 (D), HaxyOBP21 (E), HaxyOBP22 (F) and HaxyOBP28 (G).

Specifically, carbon−hydrogen bonds with tyrosine residues (like TYR138) and $\pi-\sigma$ interactions with phenylalanine residues (like PHE121, PHE141, PHE89, PHE94, PHE26 and PHE90) were frequent characteristics. The findings also show that, conventional hydrogen bonds, such as those formed with HIS91 and GLY20 (Table 2), also contributed to stabilization; however, these interactions occurred less frequently than the observed hydrophobic interactions found in some docked HIPV-OBP complexes. The conserved hydrophobic properties of OBP binding pockets are presented by the preponderance of aromatic and aliphatic residues, particularly PHE, TYR, LEU, VAL, and ILE (Figures 5−7).

The ecological role of OBPs, which are specialized for binding small, volatile, and hydrophobic odorants, is consistent with these interaction patterns observed in this study. Further, the most promising OBP−HIPV complexes for molecular dynamics simulations have been selected based on their significant docking affinities recorded on each complex as well as positive residue interactions, which also correlated the function of HIPVs in mediating predator attraction.

Molecular Dynamics

Based on binding energy (ΔG) and ligand efficiency (LE), the top-ranked docking hits (Tables 2 and S6) were used to select the six OBP−HIPV complexes shown in Table 3, Figure 4D, for molecular dynamics simulations. These complexes, which include Complex1c (HaxyOBP6−(+)-4-Carene), complex 2b (HaxyOBP9−(+)-4-Carene), Complex 4b (HaxyOBP13−1,3-cyclohexadiene-1-carboxaldehyde, 2,6,6-trimethyl-), Complex 7a (HaxyOBP19−benzene, 1-methyl-3-(1-methylethyl)−), Complex 10a (HaxyOBP23-Beta-phellandrene), and Complex 11b (HaxyOBP28−Beta-phellandrene), were selected to represent the most chemically diverse and high-scoring ligands. They were also used to see if favorable docking scores result in persistent binding under dynamic conditions. Under the same conditions, each complex underwent 100 ns explicit-solvent MDS. Using RMSD, per-residue flexibility (RMSF), radius of gyration (R_g), solvent-accessible surface area (SASA), hydrogen-bonding patterns, and interaction-fraction (contact) analyses, along with trajectory-based inspection of important pocket residues, trajectories were examined for backbone stability and binding persistence. Prior to thorough energetic decomposition and biological interpretation, this MDS-based workflow was designed to separate kinetically stable complexes from transient interactions in order to refine and prioritize docking predictions.

Root-Mean Square Deviation

The root-mean-square deviation (RMSD) profiles of the six OBP−ligand complexes over 100 ns are shown in Figure 8A. Complexes 1c, 2b, and 4b achieved stability after approximately 20 ns, with RMSD values varying between 0.6 and 0.9 nm, suggesting a moderate level of structural stability. Throughout the simulation, Complex 7a consistently displayed the lowest RMSD values (~0.4−0.6 nm), indicating a highly stable binding mode with minimal structural deviations. The enhanced stability of Complex 7a (HaxyOBP19−benzene, 1-methyl-3-(1-methylethyl)) can be attributed to persistent hydrophobic interactions between the ligand and key aromatic and aliphatic residues within the binding cavity.

https://doi.org/10.1021/acs.jafc.6c01340
J. Agric. Food Chem. XXXX, XXX, XXX−XXX

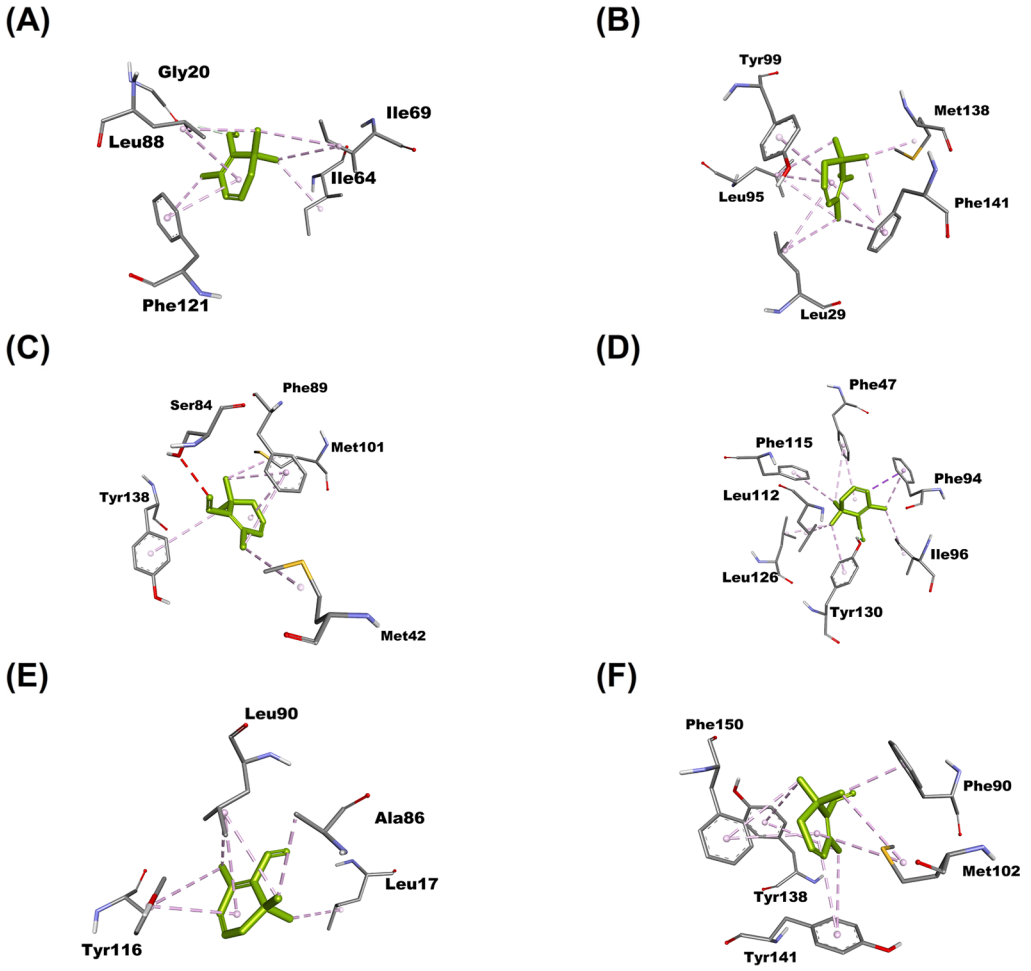

Figure 6. 3D Interaction of 1,3-cyclohexadiene-1-carboxaldehyde, 2,6,6-trimethyl with amino acids residues in HaxyOBP6 (A), HaxyOBP10 (B), HaxyOBP13 (C), HaxyOBP14 (C), HaxyOBP23 (E) and HaxyOBP28 (F).

Interaction analysis (Figures 7E and S5E) revealed sustained contacts with residues such as PHE-90 and TYR-138 throughout the 100 ns simulation, which contributed to anchoring the ligand and minimizing backbone fluctuations. These stable C−H and $\pi-\sigma$ interactions are consistent with the low RMSD and reduced RMSF observed for this complex, indicating a well-packed and conformationally restrained binding mode. In contrast, complexes 10a and 11b showed higher RMSD values, exceeding 1.0 nm after equilibration, reflecting greater conformational flexibility and reduced stability compared to the other complexes. These results indicate that Complex 7a maintained the most stable interaction with the receptor, while Complexes 10a and 11b underwent pronounced structural fluctuations. The intermediate stability observed for Complexes 1c, 2b, and 4b suggests a balance between conformational adaptability and structural conservation during the course of the simulation.

Root-Mean Square Fluctuations

The root-mean-square fluctuation (RMSF) profiles of the six OBP−ligand complexes reveal residue-specific flexibility across the protein backbone (Figure 8B). The N-terminal region (residues 1−20) showed the highest fluctuations, with Complexes 1c and 2b exceeding 1.0 nm, indicating increased mobility in this area. Beyond residue 20, fluctuations decreased substantially, with most complexes maintaining values below 0.4 nm, indicating overall structural stability of the core binding regions. Complexes 10a and 11b displayed the lowest fluctuations across the majority of residues, suggesting more rigid conformational behavior. Comparatively, Complex 1c showed localized peaks around residues 40−60 and near the C-terminal region, indicative of increased flexibility. This suggest that ligand binding stabilized most regions of the protein, with only terminal loops and select flexible segments exhibiting notable deviations. Complexes 10a and 11b demonstrated the most stable backbone dynamics, whereas Complex 1c retained higher local flexibility.

Radius of Gyration (R_g)

The Rg profiles of the six OBP-ligand complexes (Figure 8C) offer insights into the overall compactness and structural stability of the proteins during the 100 ns simulations. Complexes 1c and 10a exhibited the lowest and most stable R_g values (~1.4−1.5 nm), indicating a compact and well-folded conformation throughout the simulation. Complex 11b maintained slightly higher values (~1.6 nm) with limited fluctuations, reflecting stable packing. Complexes 2b, 4b, and 7a displayed broader variations between 1.6 and 1.9 nm, suggesting moderate flexibility and conformational adjustments. By contrast, Complex 10a showed intermittent peaks above 2.0 nm, indicating transient expansions of the protein structure. Overall, Complexes 1c and 10a maintained the most compact conformations, while 2b, 4b, and 7a exhibited higher dynamic variability. These results suggest that ligand binding

https://doi.org/10.1021/acs.jafc.6c01340
J. Agric. Food Chem. XXXX, XXX, XXX−XXX

Table 2. Binding Energy and Interacting Amino Acid Residues of the Top Ligands (HIPV) Against OBP Receptors (Bolded Residues Indicates Pi−Sigma Interaction)

OBPs	Ligand (HIPVs)	binding energy (kcal mol^{-1})	interacting residues
HaxyOBP6	Benzene, 1-methyl-3-(1-methylethyl)-	−6.5	PHE-121, ILE-69, VAL-102, PHE-98, ILE-117, VAL-81, LEU-88, ILE-64
	Beta. -Phellandrene	−6.7	VAL-102, PHE-98, PHE-121, LEU-88, ILE-64, ILE-69, ILE-117
	(+)-4-Carene	−6.8	PHE-98, ILE-117, VAL-102, ILE-69, ILE-64, LEU-88, **PHE-121**
	1,3-Cyclohexadiene-1-carboxaldehyde, 2,6,6-trimethyl-	−6.5	ILE-69, ILE-64, LEU-88, PHE-121, GLY-20
	(+)-alpha-Pinene	−6.7	ILE-69, LEU-88, ILE-64, **PHE-121**
HaxyOBP9	Benzene, 1-methyl-3-(1-methylethyl)-	−6.6	PHE-98, VAL-133, VAL-25, PHE-97, LEU-90, LEU-94, VAL-129
	(+)-4-Carene	−6.8	PHE-98, PHE-97, LEU-90, ILE-78, ILE-72, LEU-73, PHE-125, PHE-27, VAL,129, LEU-94, VAL-25
	(+)-alpha-Pinene	−6.5	VAL-129, VAL-133, PHE-125, VAL-25, PHE-98, PHE-27, PHE-97, LEU-90, ARG-93, ILE-78, LEU-94
HaxyOBP10	Beta.-Phellandrene	−6.5	LEU-29, LEU-95, TYR-99, MET-138, **PHE-141**
	1,3-Cyclohexadiene-1-carboxaldehyde, 2,6,6-trimethyl	−6.7	LEU-95, MET-138, PHE-141, LEU-29, TYR-99
HaxyOBP13	1,3-Cyclohexadiene-1-carboxaldehyde, 2,6,6-trimethyl-	−7.2	MET-42, TYR-138, MET-101, SER-84, PHE-89
	(+)-alpha-Pinene	−6.5	MET-101, HIS-104, TYR-138, **PHE-89**, LEU-105, LEU-96, PHE-141, LEU-145
HaxyOBP14	1,3-Cyclohexadiene-1-carboxaldehyde, 2,6,6-trimethyl-	−6.8	PHE-115, LEU-112, TYR-130, LEU-126, ILE-96, PHE-47, **PHE-94**
	(+)-alpha-Pinene	−6.6	LEU-87, MET-51, MET-86, ILE-72, ILE-73, VAL-54, CYS-58
HaxyOBP16	Beta. -Phellandrene	−6.8	PHE-131, ALA-128, ALA-136, MET-87, LEU-89, LEU-139, LEU-140
HaxyOBP19	Benzene, 1-methyl-3-(1-methylethyl)-	−7.7	PHE-76, VAL-139, PHE-126, TYR-129, VAL-88
	Beta. -Phellandrene	−6.6	PHE-76, TYR-129, LEU-138, HIS-91, LEU-92, VAL-137, LEU-133, VAL-88
	(+)-4-Carene	−7.3	VAL-88, TYR-129, HIS-91, LEU-133, LEU-92, LEU-138, VAL-137, VAL139, PHE-76, LEU-83
	(+)-alpha-Pinene	−6.7	VAL-88, TYR-129, LEU-138, HIS-91, VAL-139, PHE-76
HaxyOBP21	Beta. -Phellandrene	−6.5	VAL-18, LEU-5, **PHE-26**, VAL94, LEU-22, VAL-8
HaxyOBP22	Benzene, 1-methyl-3-(1-methylethyl)-	−6.5	PHE-147, MET-91, LEU-94, LEU18, PHE-26, LEU-22
	Beta. -Phellandrene	−6.7	PHE-26, LYS-23, LEU-22, LEU-18, LEU-94
HaxyOBP23	Beta. -Phellandrene	−6.7	ILE-82, LEU-90, PHE-124, **TYR-116**
	1,3-Cyclohexadiene-1-carboxaldehyde, 2,6,6-trimethyl-	−6.5	LEU-17, ALA-86, LEU-90, TYR-116
HaxyOBP28	Benzene, 1-methyl-3-(1-methylethyl)-	−7	PHE-150, **PHE-90**, TYR-138, VAL-84, MET-102
	Beta. -Phellandrene	−7.2	PHE-90, MET-102, TYR-141, TYR-138, PHE-150, VAL-149, PHE-106, HIS-105
	(+)-4-Carene	−7.2	TYR-138, MET-102, **PHE-90**, TRP-40, VAL-152, VAL-84, PHE-150, TYR-141, TYR-138
	1,3-Cyclohexadiene-1-carboxaldehyde, 2,6,6-trimethyl-	−7.1	PHE-90, PHE-150, TYR-141, TYR-138, MET-102
	(+)-alpha-Pinene	−7.1	**PHE-40**, HIS-105, MET-102, PHE-150, TYR-141, PHE-106, VAL-149, TYR-138, VAL-84

https://doi.org/10.1021/acs.jafc.6c01340
J. Agric. Food Chem. XXXX, XXX, XXX−XXX

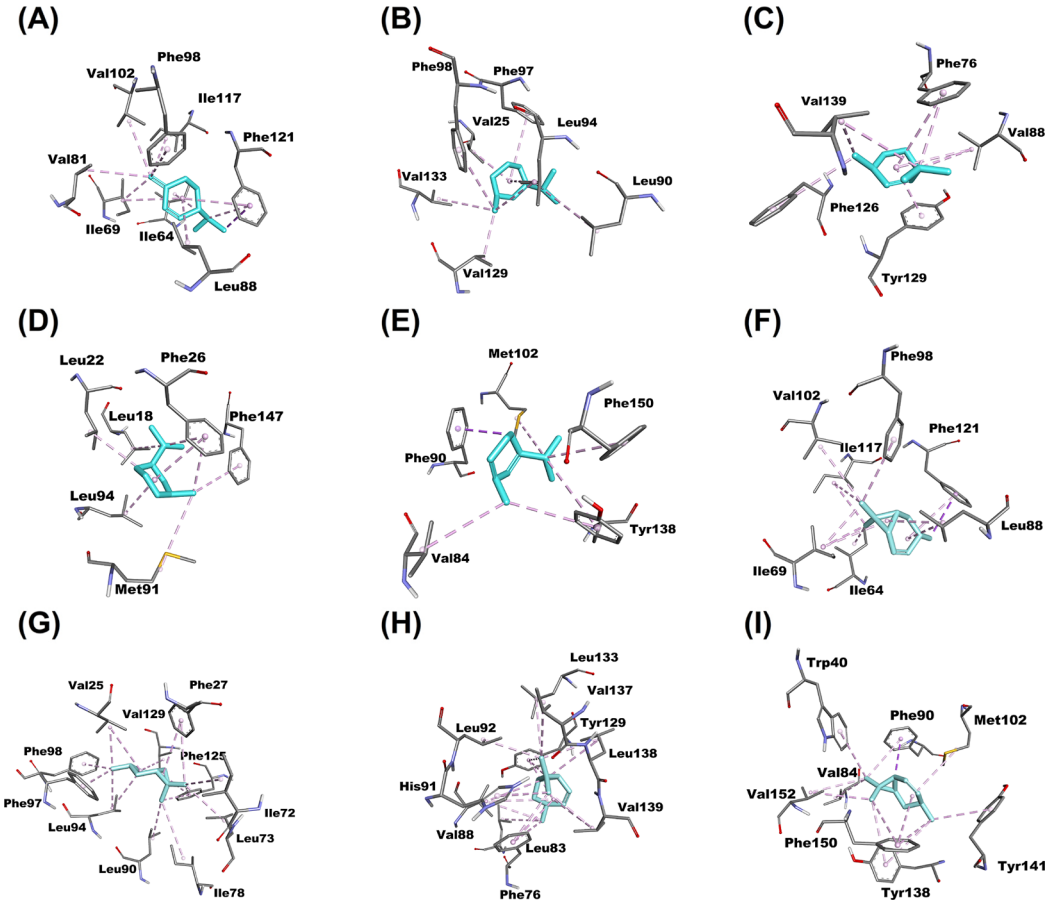

Figure 7. 3D interaction diagrams of benzene, 1-methyl-3-(1-methylethyl) with HaxyOBP9 (A), HaxyOBP6 (B), HaxyOBP28 (C), HaxyOBP22 (D) and HaxyOBP19 (E); while (F–I) indicates the Binding Interaction of (+)-4-Carene with HaxyOBP9, HaxyOBP6, HaxyOBP28, and HaxyOBP19 respectively.

Table 3. Selected Best HIPV-OBP Complexes for Molecular Dynamic Simulation Analysis OBP Ligand (HIPVs) Delta G Complexes

HaxyOBP6	(+)-4-Carene	−6.8	complex 1c
HaxyOBP9	(+)-4-Carene	−6.8	complex 2b
HaxyOBP13	1,3-cyclohexadiene-1-carboxaldehyde, 2,6,6-trimethyl-	−7.2	complex 4b
HaxyOBP19	benzene, 1-methyl-3-(1-methylethyl)-	−7.7	complex 7a
HaxyOBP23	Beta-phellandrene	−6.7	complex 10a
HaxyOBP28	Beta-phellandrene	−7.2	complex 11b

can differentially influence protein compactness, with certain complexes favoring more stable folded states and others permitting greater structural flexibility.

Solvent-Accessible Surface Area

The solvent-accessible surface area (SASA) analysis (Figure 8D) revealed differences in solvent exposure and compactness among the six OBP–ligand complexes over 100 ns simulations. Complexes 1c and 10a exhibited the lowest SASA values (~730–800 nm^2), indicating reduced solvent exposure and more compact conformations. Complex 2b stabilized around ~850 nm^2, whereas Complex 4b and 11b maintained intermediate values in the range of 880–920 nm^2. Complex 7a consistently displayed the highest SASA (>950 nm^2), reflecting greater solvent exposure and a less compact structural arrangement. The lower SASA values observed for Complexes 1c and 10a suggest tighter packing and stronger stabilization, while the higher SASA in Complex 7a indicates a looser conformation and greater interaction with the solvent environment.

Protein–Ligand Interactions

The interaction fraction analysis of the OBP–ligand complexes (Figure 9A–F) highlights differences in binding stabilization mechanisms. Hydrophobic contacts were the dominant interaction type across all complexes, consistent with the predominantly hydrophobic cavity of OBP. In Complex 1c (Figure 8A), PHE-118 and PHE-121 formed persistent hydrophobic interactions, anchoring the ligand within the pocket. Complex 2b (Figure 9B) displayed fewer stable contacts overall, although PHE-97 and PHE-119 contributed notably to ligand stabilization. Complex 4b (Figure 9C) exhibited a broader interaction network that combined hydrophobic contacts with hydrogen bonds and water bridges. This diversity of interactions suggests enhanced binding stability, in line with the lower RMSD values and reduced

https://doi.org/10.1021/acs.jafc.6c01340
J. Agric. Food Chem. XXXX, XXX, XXX–XXX

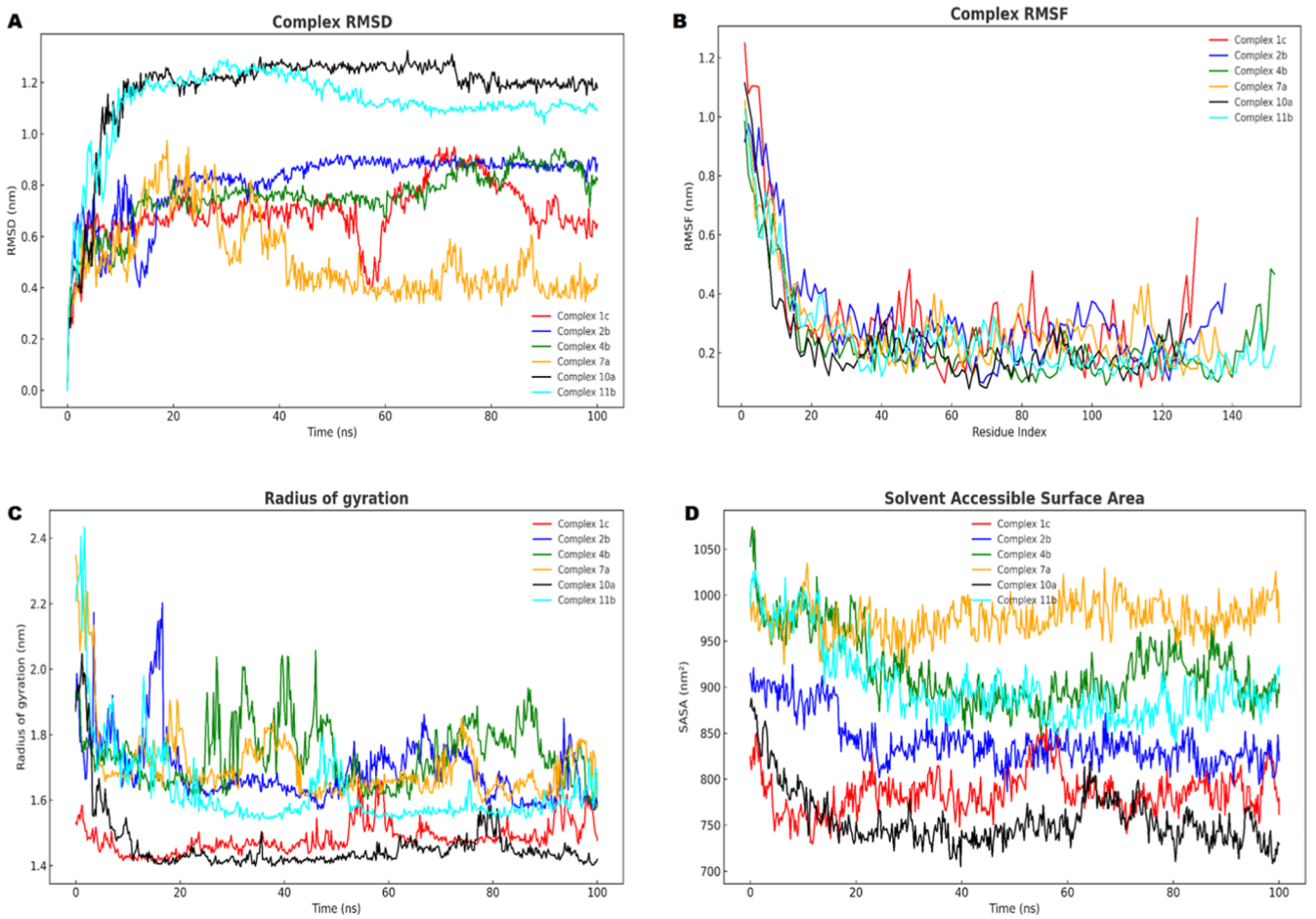

Figure 8. Root-mean-square deviation (RMSD) profiles of six OBP−ligand complexes over 100 ns molecular dynamics simulations (A). Complexes 1c, 2b, and 4b display moderate stability with RMSD values stabilizing around 0.6−0.9 nm, whereas Complex 7a remains the most stable with values near 0.4−0.6 nm. In contrast, Complexes 10a and 11b exhibit higher deviations (>1.0 nm), reflecting reduced structural stability. Root-mean-square fluctuation (RMSF) of backbone residues for six OBP−ligand complexes (B). The N-terminal residues exhibit the highest fluctuations, particularly in Complexes 1c and 2b, while the central regions remain stable (<0.4 nm). Complexes 10a and 11b show the lowest overall flexibility, whereas Complex 1c displays localized peaks of higher mobility, especially near residues 40−60 and the C-terminal region. Radius of gyration (R_g) of six OBP−ligand complexes (C). Complexes 1c and 10a show the lowest and most stable R_g values (∼1.4−1.5 nm), indicating compact conformations, whereas Complexes 2b, 4b, and 7a exhibit higher variability (∼1.6−1.9 nm). Complex 11b remains moderately stable (∼1.6 nm), while transient peaks in Complex 10a reflect brief conformational expansions. Solvent-accessible surface area (SASA) of six OBP−ligand complexes (C). Complexes 1c and 10a exhibit the lowest SASA values (∼730−800 nm^2), indicating compact structures with reduced solvent exposure. Complexes 2b, 4b, and 11b maintain intermediate solvent exposure (∼850−920 nm^2), whereas Complex 7a shows the highest SASA (>950 nm^2), reflecting a less compact conformation.

residue fluctuations observed for this complex. Similarly, Complex 10a (Figure 8E) combined polar and nonpolar contacts, reinforcing its stable profile evidenced by compact Rg values and reduced solvent exposure in SASA analysis (Figure 9D).

By contrast, complexes 7a and 11b (Figure 9D,F) were dominated almost exclusively by hydrophobic interactions, with TRP-25, PHE-59, and PHE-121 as major contributors. The limited diversity of contacts may account for their higher SASD variability and larger SASA, indicating weaker packing and less favorable stabilization compared to complexes 4b and 10a. Taken together, the interaction analysis corroborates the structural stability trends observed in RMSD, RMSF, R_g, and SASA (Figure 8A−D). Ligands capable of establishing a balanced network of hydrophobic and polar interactions—particularly complexes 4b and 10a, emerge as the most promising candidates for sustained OBP binding. Hence, based on integrated docking, ligand efficiency, interaction pattern analysis, and molecular dynamics simulations, HaxyOBP13, HaxyOBP19, and HaxyOBP23 emerged as the most relevant candidates for HIPV recognition, with HaxyOBP28 showing strong affinity toward specific sesquiterpenes.

In-Vitro Binding Assay. First, the HaxyOBP13, HaxyOBP19 and HaxyOBP23 recombinant proteins were prepared by a prokaryotic expression system and affinity chromatography. Subsequently, the N- terminal His-tag was cleaved using thrombin. The SDS-PAGE analysis revealed a single band with the expected relative molecular weight for HaxyOBP proteins tested (Figure S7). However, the binding affinities of the fluorescent probe *N*-phenyl-1-naphthylamine (1-NPN) to the three recombinant proteins (HaxyOBP13, HaxyOBP19, and HaxyOBP23) were determined using fluorescence-based binding assays (Figure 10A). According to this result, the proteins were found to bind strongly to the 1-NPN probe, with calculated dissociation constants (K_d) of 10.77 ± 1.81 μM 10.77 ± 1.81 μM for HaxyOBP13, 14.58 ± 1.08 μM for

https://doi.org/10.1021/acs.jafc.6c01340
J. Agric. Food Chem. XXXX, XXX, XXX−XXX

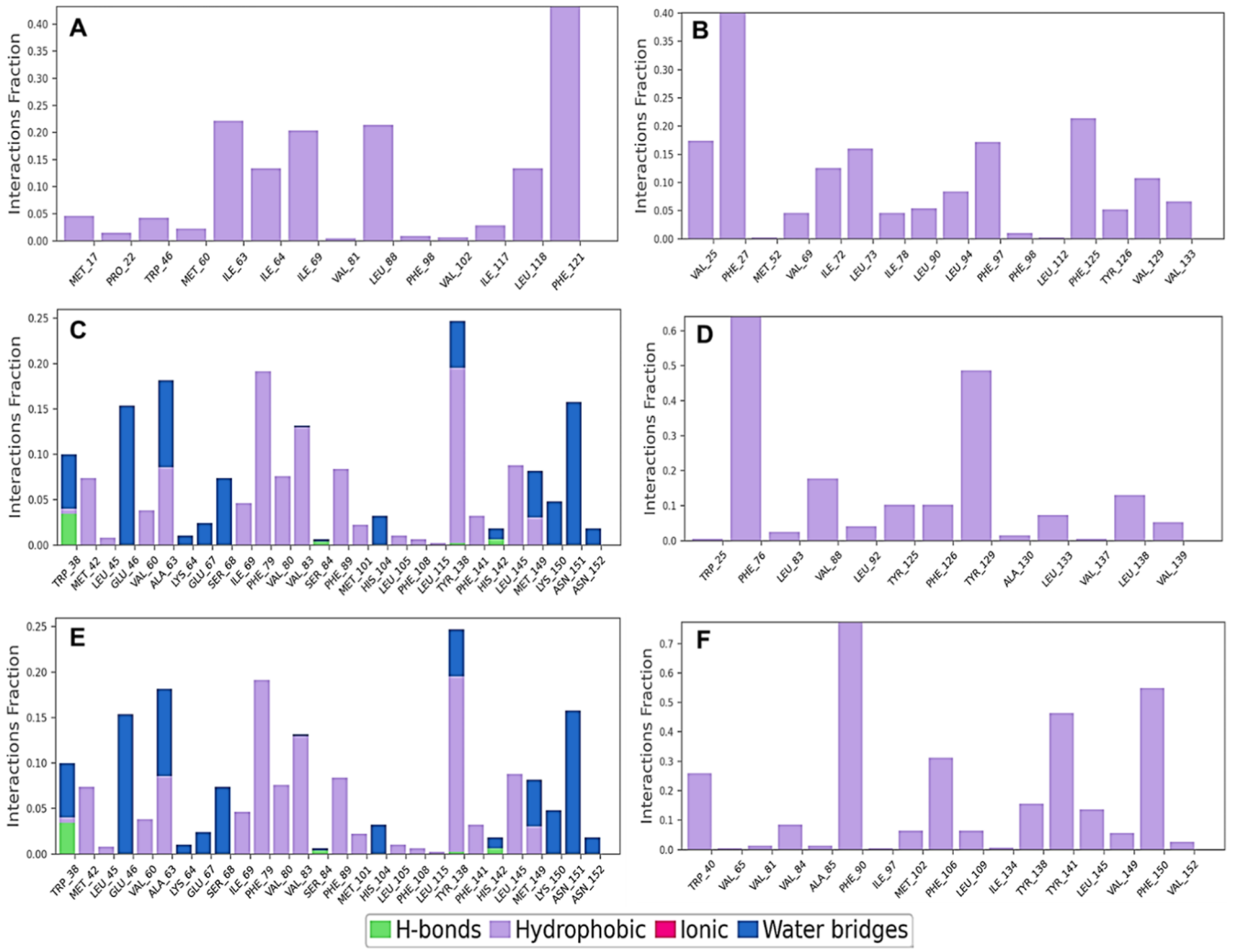

Figure 9. Protein−ligand interaction profiles of OBP complexes over the course of MD simulations. Interaction fractions are shown for key residues in each complex: (A) complex 1c, (B) complex 2b, (C) complex 4b, (D) complex 7a, (E) complex 10a, and (F) complex 11b. Interaction types are color-coded as hydrogen bonds (green), hydrophobic (purple), ionic (pink), and water bridges (blue).

HaxyOBP19, and 6.45 ± 0.267 μM for HaxyOBP23. The strong binding affinity, particularly for HaxyOBP23, indicated that 1-NPN was a suitable probe for subsequent competitive binding experiments.

Further, competitive binding assays were then performed to assess the binding of specific ligands to these proteins, using 1-NPN as the fluorescent reporter (Figure 10B). The concentration of each competitor ligand that reduced the initial fluorescence intensity by half (IC_{50}) was determined and used to calculate the dissociation constants (K_i) (Figure 10C). For HaxyOBP13, the ligand 1,3-cyclohexadiene-1-carboxaldehyde, 2,6,6-trimethyl exhibited a K_i of 3.13 ± 0.67 μM. HaxyOBP19 showed a K_i of 3.01 ± 0.41 μM for benzene, 1-methyl-3-(1-methylethyl). The ligand beta-phellandrene bound most strongly to HaxyOBP23, with a calculated K_i of 1.97 ± 0.26 μM, which was the highest affinity observed among all tested interactions.

DISCUSSION

This study offers a computational framework to evaluate HIPV−OBP interactions relevant to pest control. The integration of docking, LE, and dynamic simulation supports the feasibility of developing semiochemical-based attractants for *H. axyridis*. In order to investigate how herbivore-induced plant volatiles (HIPVs) might influence the foraging behavior of *H. axyridis*, a significant predator of *T. absoluta*, our study integrated behavioral assays with in silico docking. Although the present study does not establish direct behavioral causality of individual HIPVs but provides a mechanistically grounded prioritization framework linking plant-emitted volatiles to predator olfactory recognition, we discovered that adult beetles are attracted to volatiles from tomatoes infested with *T. absoluta* and that several tomato HIPVs bind strongly to particular *H. axyridis* OBPs. Despite that males and females were pooled in the behavioral assays, the study focused on general prey-location responses; sex-specific olfactory preferences merit further investigation.

However, a previous study has confirmed that insect antennae are rich in odorant-binding proteins, which solubilize and deliver volatile odorants to olfactory receptors.[32] Furthermore, OBPs have been emphasized as important participants in semiochemical detection and as practical targets for locating compounds with behavioral activity.[32,33] For instance, our docking analyses revealed that *H. axyridis* OBPs (specifically OBP6, OBP9, OBP10, OBP13, OBP14, OBP28, etc.) had a high affinity (−6.5 to −7.4 kcal mol^{-1}) for

https://doi.org/10.1021/acs.jafc.6c01340
J. Agric. Food Chem. XXXX, XXX, XXX−XXX

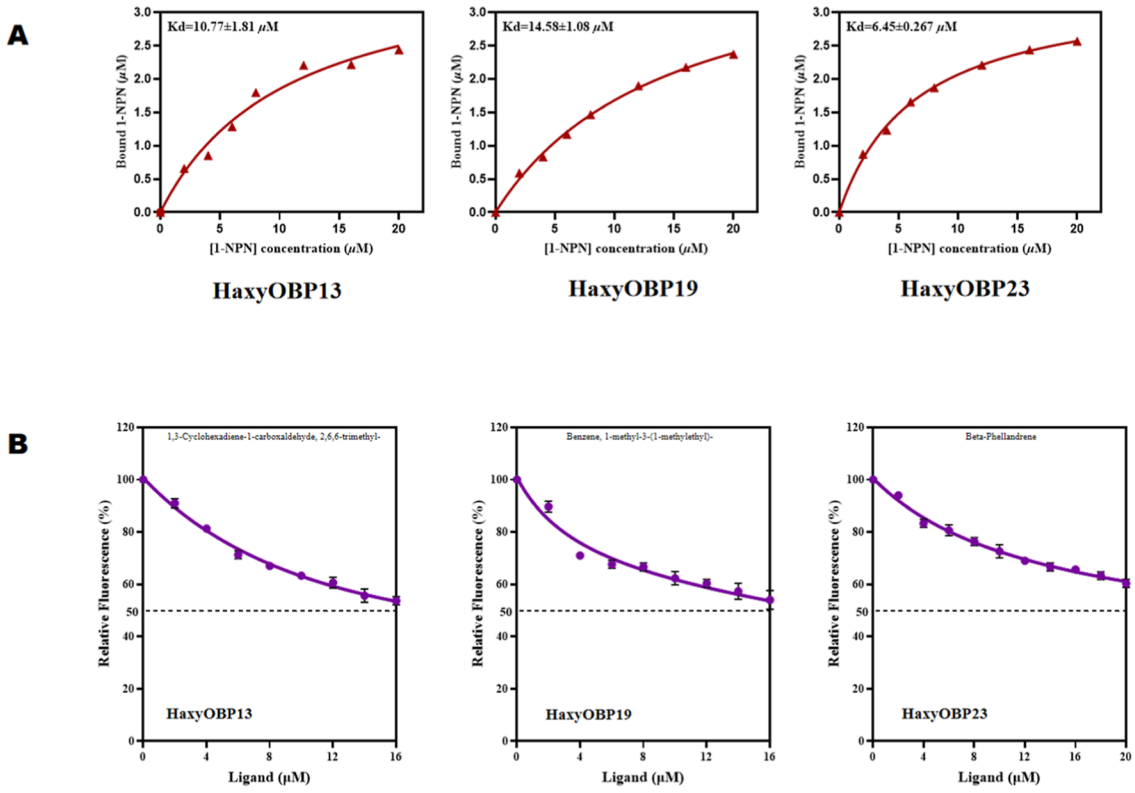

C

	Ligand	IC_{50} (μM)	K_i (μM)	$1/K_i$
HaxyOBP13	1,3-Cyclohexadiene-1-carboxaldehyde, 2,6,6-trimethyl-	19.74±0.58	3.13±0.67	0.319
HaxyOBP19	Benzene, 1-methyl-3-(1-methylethyl)-	19.47±1.25	3.01±0.41	0.332
HaxyOBP23	Beta-Phellandrene	27.57±0.83	1.97±0.26	0.508

Figure 10. Binding affinity of the fluorescent probe 1-NPN and target volatile ligands to HaxyOBP13, HaxyOBP19, and HaxyOBP23. (A) Saturation binding curves and Scatchard plots showing the binding of 1-NPN to the three recombinant HaxyOBPs. The dissociation constant (K_d) values were determined for each protein. (B) Competitive binding curves illustrating the displacement of the fluorescent probe 1-NPN (10 μM) by increasing concentrations of target ligands (1,3-cyclohexadiene-1-carboxaldehyde, 2,6,6-trimethyl- for HaxyOBP13; benzene, 1-methyl-3-(1-methylethyl)- for HaxyOBP19; Beta-phellandrene for HaxyOBP23). (C) A summary table of the calculated half-maximal inhibitory concentration (IC_{50}), dissociation constant (K_i), and reciprocal dissociation constant ($1/K_i$) values for the specific ligand-OBP interactions. Data points represent the mean ± standard error of the mean (SEM) from replicate experiments.

monoterpenes like (+)-4-carene, (+)-α-pinene, and β-phellandrene. Collectively, these substances make up a significant portion of the HIPV bouquet and are important constituents of the volatile blend released by tomatoes infested with *T. absoluta*.[34] In line with the widely accepted discoveries that OBPs bind and shield volatile odorants in the sensillum lymph prior to receptor activation, the docking models showed hydrophobic binding pockets formed by conserved residues (including Phe, Leu, Val, Tyr, and Ile) that interact with these hydrophobic ligands.[32,33] The strong predicted binding indicates that these monoterpenes are likely natural ligands for *H. axyridis* OBPs, even though in silico affinity estimates represent an approximation.

The phylogenetic clustering of HaxyOBPs shows that a number of paralog groups maintain high sequence conservation, pointing to conserved structural motifs in their ligand-binding pockets. When kinetically stable and high-affinity complexes (from docking/MDS) colocalize in the same clade, it suggests that similar chemical recognition is supported by clade-level pocket architecture. For instance, high ligand efficiency of HaxyOBP19 for benzaldehyde (Figure 5B) and exceptionally strong binding of HaxyOBP28 to the sesquiterpene ($\Delta G = -8.2$ kcal·mol^{-1}) are most instructive when viewed in their phylogenetic context (Figure 2A,B). This is because closely related paralogs may be expected to exhibit similar specificity,[35] which would indicate a clade-level recognition of these chemical classes.

On the other hand, OBPs from different clades may exhibit similar or identical ligand affinities (for example, β-isomethyl ionone binding to HaxyOBP1, HaxyOBP6, and HaxyOBP7), as illustrated in Figures 2B and 3A. The observation that these HaxyOBPs exhibit affinity toward β-isomethyl ionone suggests a degree of functional redundancy within the olfactory system of *H. axyridis*. Such redundancy may enhance olfactory reliability under ecologically realistic conditions, where predators encounter complex and fluctuating volatile blends emitted by tomato plants under herbivore attack. By distributing detection of key HIPVs across several OBPs, *H. axyridis* may reduce the risk of signal loss due to environmental noise or variable ligand concentrations. Alternatively, this redundancy may reflect evolutionary divergence following OBP gene expansion, whereby closely related OBPs retain overlapping ligand spectra while gradually specializing toward distinct chemical features. These nonmutually exclusive

https://doi.org/10.1021/acs.jafc.6c01340
J. Agric. Food Chem. XXXX, XXX, XXX−XXX

mechanisms highlight how OBP multiplicity can support both robustness and flexibility in odor-guided foraging behavior. A structural explanation for the observed docking/MDS results can be found by mapping pocket residues onto the alignment, which indicates that aromatic and aliphatic residues (PHE, TYR, LEU, VAL, and ILE) are frequently conserved in clades exhibiting stable hydrophobic recognition.

Prioritization is practically guided by the phylogeny. Close paralogs in well-supported clades, such as OBPs with low binding energy and low RMSD in MDS, can be effectively screened as predicted binders, and these clades are excellent candidates for recombinant expression and ligand-binding assays (K_d determination). It is crucial to confirm functional claims through experiments when there is insufficient bootstrap support. In designing lures for field biocontrol, the phylogenetic pattern suggests a strategy that involves attracting both a variety of chemical ligands (to appeal across different groups) and specific ligands for particular clades for targeted, highly effective attractants.[35]

However, ligand-efficiency analysis has reprioritized specific HIPV candidates by prioritizing small and atom-efficient ligands with high binding per heavy atom. This has helps to identify compact ligands with favorable physicochemical properties, mitigating the bias toward larger molecules often seen when ranking solely by affinity. This metric is commonly employed in ligand selection workflows; hence, it is still a useful tool for hit selection in molecular screening, despite its drawbacks and reliance on the definition and units of affinity.[36] Our behavioral assays with *H. axyridis* demonstrated an attraction to volatiles emitted by infested plants, thereby establishing an empirically supported connection between the binding potential of olfactory binding proteins (OBPs) and the orientation of predators. This supports the notion that selected herbivore-induced plant volatiles (HIPVs) can function as biologically significant semiochemicals to attract predators within agricultural systems. The combined docking and LE results have direct ecological relevance. Herbivore-induced plant volatiles (HIPVs) are indirect defenses that attract natural enemies, enabling predators and parasitoids to locate hosts.

Additionally, our behavioral bioassays confirmed that *H. axyridis* uses HIPVs as cues for foraging. The odor of tomato plants infested with *T. absoluta* was significantly preferred by adults in Y-tube olfactometer trials compared to uninfested controls (e.g., choice ratios of 2:1 in favor of infested) (Figure 1). This result is consistent with earlier findings that plants infested by herbivores attract predatory coccinellids.[37] In this regard, Xu et al. (2023) showed that *H. axyridis* strongly responds to the volatiles of *V. negundo* that has been infested by aphids and identified particular HIPVs that produced strong olfactory responses, such as sclareol, eucalyptol, nonanal, and α-terpineol. In the present case, the tomato infested with *T. absoluta* probably releases higher concentrations of terpenoid volatile organic compounds (VOCs) like β-phellandrene, α-pinene, and others, which act as important attractants.[34,37] In accordance with the function of OBPs in odor transport,[32] the convergence of docking and behavior indicates that OBPs in *H. axyridis*' antenna absorb the odor molecules when it comes into contact with these HIPVs, thereby initiating orientation toward the source. Our findings thus is supported by the phenomenon that *H. axyridis* OBPs encode sensitivity to herbivore-related plant cues by establishing a mechanistic connection between molecular binding and ecological response.

Additionally, the strong binding affinities (K_i) determined through in vitro competitive binding assays for ligands like beta-phellandrene (K_i of 1.97 ± 0.26 μM 1. Nine 7 ± 0. Two 6 μM) to specific OBP receptors (HaxyOBP23) further provide the molecular foundation for the observed attraction and also support our stated finding from in-silico predictions. The result from the molecular docking simulations (Figure 3A−D) strongly correlates with these in vitro findings, showing high binding energy (Figures 3A and 4D) for the ligands that exhibited the lowest K_i values in the experimental assays. This synergy between computational (docking/MDS) and experimental data (in vitro binding) validates the accuracy of our predictions regarding key odorant−protein interactions. These specific, high-affinity interactions suggest that *H. axyridis* olfactory systems are finely tuned to detect the *T. absoluta* induced VOCs, effectively translating a molecular recognition event into a significant behavioral response (predator attraction). Thus, the successful identification of potent VOCs and their corresponding binding proteins offers a promising strategy for enhancing the biological control of *T. absoluta*. By developing synthetic blends that mimic the most attractive HIPVs, we can potentially increase predator populations in tomato fields and improve the efficacy of integrated pest management (IPM) programs.

Ecologically, the ability of *H. axyridis* to detect and respond to plant odors produced by herbivores is an indirect plant defense mechanism.[37,38] Terpenoids and other volatile organic compounds (VOCs) that are uncommon or present in trace amounts in healthy plants are frequently released during herbivore attacks.[34,37] Predators can identify areas of infestation via these HIPVs, which serve as reliable signals of prey presence in the environment. Several *H. axyridis* OBPs can bind the same monoterpenes with similar affinity, according to our docking results, indicating some redundancy or broad tuning in the OBP repertoire. The robustness of odor detection in complex odor landscapes can be enhanced by OBPs' frequent overlapping ligand spectra in other insects.[32,33] Simultaneously, slight variations in binding residues among OBPs, as observed in our models, might enable *H. axyridis* to distinguish between related volatiles or concentration shifts. However, we observe that many HIPVs (such as β-phellandrene and α-pinene) are not specific to *T. absoluta* infestations but rather are released by a variety of plant species.[39,40] Although these cues are beneficial, they are generalist signals, meaning that nontarget insects—such as other predators or even pests—may also react. Both downstream neural processing and OBP binding are necessary for the specificity of behavioral attraction. High OBP-binding affinity in practice indicates that these substances will probably trigger the olfactory system of predator to produce detectable signals.[32,33]

Our results point to possible semiochemicals for use in attractant lures aimed at *T. absoluta* agroecosystems from the standpoint of pest management. Here, we envision an analogous strategy to attract and enhance predators, even though attract-and-kill is typically used to expose pests to a lethal agent. Predation on *T. absoluta* may increase if synthetic dispensers of the main HIPVs, particularly the monoterpenes β-phellandrene, 1,3-cyclohexadiene-1-carboxaldehyde-2,6,6-trimethyl (safranal), and aromatic hydrocarbon benzene,1-methyl-3-(1-kethyl) or *m-Cymene*, "pull" *H. axyridis* into

https://doi.org/10.1021/acs.jafc.6c01340
J. Agric. Food Chem. XXXX, XXX, XXX−XXX

tomato fields or particular trap plants. This is similar to a pull element in a push−pull strategy; predators are attracted to odor lures (pull), while pests may be simultaneously repelled by other methods (push). However, HIPVs are frequently used in conservation biological control to enlist natural enemies.[37,38] To improve enemy efficacy, for instance, controlled release of HIPVs in the field has been proposed.[38] In order to provide persistent odor plumes, the compounds found here could be used in slow-release dispensers or nanofibre mats.[41] Rapid volatile loss from the field will require careful formulation; coformulation with polymers or nanoencapsulation may stabilize emission, as has been done with pheromones and essential oils.[41] In addition, the potential for HIPVs to attract nontarget organisms, including herbivores such as *T. absoluta* or other arthropods, must be carefully evaluated. Selective formulation, optimized release rates, and blend composition may mitigate such risks by favoring predator responsiveness over herbivore attraction.[42,43] Integrating these formulation strategies with ecological risk assessment will be essential for translating HIPV-based lures into effective and sustainable biological control tools.

Concurrently, blends of complementary attractants have been developed for *T. absoluta*. For example, another study found that, tomato volatiles that are either repellent (*trans*-nonadienal, *trans*-2-nonenal) or attractive (e.g., 1-nonanol, ethyl octanoate) to female *T. absoluta*.[44] They also demonstrated that these compounds could be used in lure-and-avoid schemes. As a result, a combined approach may employ particular HIPVs to attract predators and distinct volatiles (or trap plants) to entice pests into or away from lethal traps. Other systems have effectively used such integrated push−pull schemes, where "pull" stimuli attract in natural enemies and "push" stimuli deter or repel pests.[38,41]

However, given the complexity of field deployment, we must temper our enthusiasm. Insect responses can be modulated by background odor, climatic variation, and ecological context, so laboratory attraction does not always translate to open-field efficacy.[38,41] Therefore, to measure *H. axyridis* attraction under real-world scenarios, future research should test the candidate HIPV blends in greenhouse or field-cage trials. The selection of lure components would be improved by competitive binding assays and electrophysiological assays (such as antennal recording), which would further confirm which OBPs bind which volatiles the strongest. The effects of these lures on nontarget organisms and *T. absoluta* should also be evaluated. For instance, it is critical that HIPV lures do not unintentionally attract in *T. absoluta* moths (if they react to monoterpenes) or other undesirable insects. Favoring biological control agents within the local insect community.

In a nutshell, our behavioral and in silico modeling suggest that *H. axyridis* can detect certain tomato HIPVs through its OBPs and can stimulate attraction in olfactometer tests. These HIPVs, which are mostly monoterpenes released when herbivores induce attack, are cues that have ecological significance and show promise as components of semiochemical lures. Pest managers could increase natural predation by using these volatiles to develop innovative, environmentally friendly attractant devices to attract *H. axyridis* into crops infested with *T. absoluta*. Finding the odor signatures that link plants, pests, and predators is a crucial first step in managing tomato leafminers sustainably, and our findings set the foundation for such push−pull and attractant-based tactics.[38,44]

Behavioral assays and complementary in silico analyses converge to identify specific OBP−HIPV pairs that plausibly mediate *H. axyridis* attraction to *T. absoluta*−infested tomato. Our findings demonstrate that infestation significantly enhances Tomato attractiveness, with *H. axyridis* being 82% more likely to select infested *T. absoluta*-infested Tomato plant, reflecting a medium but biologically meaningful effect. Docking and ligand-efficiency ranking revealed a number of high-affinity pairs, including the sesquiterpene−HaxyOBP28 complex, strong β-isomethyl-ionone binding to HaxyOBP1/6/7, and high LE for HaxyOBP19−benzaldehyde. By separating kinetically stable complexes (HaxyOBP19- benzene,1-methyl-3-(1-methylethyl), HaxyOBP13−1,3-cyclohexadiene-1-carboxaldehyde,2,6,6-trimethyl, HaxyOBP6-(+)-4-Carene and HaxyOBP23-Beta-Phellandrene as additional sustained binders) from less reliable binders, 100 ns MDS improved these predictions. According to interaction profiling, the structural foundation for ligand recognition is conserved hydrophobic pockets that are dominated by aromatic and aliphatic residues (PHE, TYR, LEU, VAL, and ILE). These findings collectively offer a prioritised list of OBP−HIPV candidates for empirical validation and attractant formulation; field testing and lure-development research should allow for the implementation of focused, OBP-informed lure strategies to improve sustainable biocontrol of *T. absoluta* and increase recruitment of *H. axyridis*.

While molecular docking and molecular dynamics simulations provide valuable insights into potential OBP−HIPV interactions, several limitations should be acknowledged. The OBP structures used in this study represent static or limited dynamic conformations and may not fully capture the complete range of structural flexibility exhibited by OBPs in vivo. Additionally, post-translational modifications, such as phosphorylation or glycosylation, which could influence ligand binding or protein stability, were not considered in the in silico models or recombinant proteins. Consequently, the binding affinities reported here should be interpreted as predictive estimates rather than absolute measures. Nonetheless, the convergence of in silico analyses with fluorescence competitive binding assays supports the biological relevance of the identified OBP−HIPV interactions and provides a robust foundation for future in vivo and field-based validation.

■ ASSOCIATED CONTENT

Data Availability Statement

Data not provided in the manuscript is available upon request to the corresponding author.

Supporting Information

The Supporting Information is available free of charge at https://pubs.acs.org/doi/10.1021/acs.jafc.6c01340.

Tables S1−S6 (HIPVs with PubChem and CAS identifiers; structural quality metrics of modeled HaxyOBPs; binding poses and interacting residues; behavioral assay statistics; docking binding energies; molecular dynamics-selected complexes); Figures S1−S7 (Ramachandran plots; two- and three-dimensional ligand−protein interaction diagrams; SDS-PAGE analysis of recombinant HaxyOBPs) (PDF)

https://doi.org/10.1021/acs.jafc.6c01340
J. Agric. Food Chem. XXXX, XXX, XXX−XXX

AUTHOR INFORMATION

Corresponding Author

Youming Hou − *State Key Laboratory of Ecological Pest Control for Fujian and Taiwan Crops; Key Laboratory of Biopesticides and Chemical Biology, Ministry of Education; College of Plant Protection, Fujian Agriculture and Forestry University, Fuzhou 350002, China;* orcid.org/0000-0001-7984-9688; Email: ymhou@fafu.edu.cn

Authors

Tijjani Mustapha − *State Key Laboratory of Ecological Pest Control for Fujian and Taiwan Crops; Key Laboratory of Biopesticides and Chemical Biology, Ministry of Education; College of Plant Protection, Fujian Agriculture and Forestry University, Fuzhou 350002, China; Department of Plant Biology, Federal University Dutse, Dutse 7156, Nigeria;* orcid.org/0000-0001-6366-6510

Youdan Zhang − *State Key Laboratory of Ecological Pest Control for Fujian and Taiwan Crops; Key Laboratory of Biopesticides and Chemical Biology, Ministry of Education; College of Plant Protection, Fujian Agriculture and Forestry University, Fuzhou 350002, China*

Jianquan Yan − *State Key Laboratory of Ecological Pest Control for Fujian and Taiwan Crops; Key Laboratory of Biopesticides and Chemical Biology, Ministry of Education; College of Plant Protection, Fujian Agriculture and Forestry University, Fuzhou 350002, China*

Huatao Tang − *State Key Laboratory of Ecological Pest Control for Fujian and Taiwan Crops; Key Laboratory of Biopesticides and Chemical Biology, Ministry of Education; College of Plant Protection, Fujian Agriculture and Forestry University, Fuzhou 350002, China*

Zhujun Wang − *State Key Laboratory of Ecological Pest Control for Fujian and Taiwan Crops; Key Laboratory of Biopesticides and Chemical Biology, Ministry of Education; College of Plant Protection, Fujian Agriculture and Forestry University, Fuzhou 350002, China*

Sheng-Yen Wu − *State Key Laboratory of Ecological Pest Control for Fujian and Taiwan Crops; Key Laboratory of Biopesticides and Chemical Biology, Ministry of Education; College of Plant Protection, Fujian Agriculture and Forestry University, Fuzhou 350002, China*

Abdul Basit − *State Key Laboratory of Ecological Pest Control for Fujian and Taiwan Crops; Key Laboratory of Biopesticides and Chemical Biology, Ministry of Education; College of Plant Protection, Fujian Agriculture and Forestry University, Fuzhou 350002, China*

Yassir Boulaamane − *Laboratory of Innovative Technologies, National School of Applied Sciences of Tangier, Abdelmalek Essaadi University, Tetouan 93000, Morocco*

Anshuman Chandra − *School of Physical Sciences, Jawaharlal Nehru University, New Delhi 110067, India*

Mai-Abba Ishiyaku Abdullahi − *Department of Plant Biology, Federal University Dutse, Dutse 7156, Nigeria*

Moazam Hyder − *State Key Laboratory of Ecological Pest Control for Fujian and Taiwan Crops; Key Laboratory of Biopesticides and Chemical Biology, Ministry of Education; College of Plant Protection, Fujian Agriculture and Forestry University, Fuzhou 350002, China*

Complete contact information is available at: https://pubs.acs.org/10.1021/acs.jafc.6c01340

Author Contributions

[⊥]T.M. and Y.Z. contributed equally to this work. **Tijjani Mustapha, Jianquan Yan, Youdan Zhang& Huatao Tang**: Conceptualization; Methodology; Molecular docking; Investigation; Data curation; Formal analysis and phylogenetic analysis; **Zhujun Wang, Sheng-Yen Wu**: Methodology; Formal Analysis; Data validation. **Abdul Basit& Moazam Hyder**: Data analysis; Visualization; Writing—review and editing. **Yassir Boulaamane, Anshuman Chandra& Mai-Abba Ishiyaku Abdullahi**: Investigation; Formal analysis; Contribution to molecular dynamic simulation; Resources and Validation. **Youming Hou**: Funding acquisition; Conceptualization; Supervision; Project administration; Writing—review and editing.

Funding

This work was funded by the National Natural Science Foundation of China (U22A20489,32361143791).

Notes

The authors declare no competing financial interest.

REFERENCES

(1) Buragohain, P.; Saikia, D. K.; Sotelo-Cardona, P.; Srinivasan, R. Development and validation of an integrated pest management strategy against the invasive South American tomato leaf miner, Tuta absoluta in South India. *Crop Prot.* **2021**, *139*, 105348.

(2) Pandey, K. A.; Kumar, A.; Dinesh, K.; Varshney, R.; Dutta, P. The hunt for beneficial fungi for tomato crop improvement−Advantages and perspectives. *Plant Stress* **2022**, *6*, 100110.

(3) Pandey, M.; Bhattarai, N.; Pandey, P.; Chaudhary, P.; Katuwal, D. R.; Khanal, D. A review on biology and possible management strategies of tomato leaf miner, Tuta absoluta (Meyrick), Lepidoptera: Gelechiidae in Nepal. *Heliyon* **2023**, *9* (6), No. e16474.

(4) González-Cabrera, J.; Mollá, O.; Montón, H.; Urbaneja, A. Efficacy of Bacillus thuringiensis (Berliner) in controlling the tomato borer, Tuta absoluta (Meyrick) (Lepidoptera: Gelechiidae). *BioControl* **2011**, *56* (1), 71−80.

(5) Jallow, M. F. A.; Dahab, A. A.; Albaho, M. S.; Devi, V. Y. Efficacy of Nesidiocoris tenuis (Hemiptera: Miridae) and Bacillus thuringiensis (Berliner) for controlling Tuta absoluta (Lepidoptera: Gelechiidae) in greenhouse tomato crops under Kuwait hot desert climate. *Int. J. Pest Manage.* **2024**, *70* (4), 1149−1159.

(6) Mollá, O.; González-Cabrera, J.; Urbaneja, A. The combined use of Bacillus thuringiensis and Nesidiocoris tenuis against the tomato borer Tuta absoluta. *BioControl* **2011**, *56* (6), 883−891.

(7) Chen, L.; Li, X.; Zhang, J.; He, T.; Huang, J.; Zhang, Z.; Wang, Y.; Hafeez, M.; Zhou, S.; Ren, X.; Hou, Y.; Lu, Y. Comprehensive Metabolome and Volatilome Analyses in Eggplant and Tomato Reveal Their Differential Responses to Tuta absoluta Infestation. *Front. Plant Sci.* **2021**, *12*, 757230.

(8) Birhan, A. Tomato leafminer [(Tuta absoluta Meyrick) (Lepidoptera: Gelechiidae)] and its current ecofriendly management strategies: A review. *J. Agric. Biotechnol. Sustainable Dev.* **2018**, *10* (2), 11−24.

(9) Xu, Q.; Wu, C.; Xiao, D.; Jin, Z.; Zhang, C.; Hatt, S.; Guo, X.; Wang, S. Ecological function of key volatiles in Vitex negundo infested by Aphis gossypii. *Front. Plant Sci.* **2023**, *13*, 1090559.

(10) Cai, Z.; Ouyang, F.; Su, J.; Zhang, X.; Liu, C.; Xiao, Y.; Zhang, J.; Ge, F. Attraction of adult Harmonia axyridis to volatiles of the insectary plant Cnidium monnieri. *Biol. Control* **2020**, *143*, 104189.

(11) De Backer, L.; Bawin, T.; Schott, M.; Gillard, L.; Markó, I. E.; Francis, F.; Verheggen, F. Betraying its presence: identification of the chemical signal released by Tuta absoluta-infested tomato plants that guide generalist predators toward their prey. *Arthropod-Plant Interact.* **2017**, *11* (2), 111−120.

(12) Silva, D. B.; Weldegergis, B. T.; Van Loon, J. J. A.; Bueno, V. H. P. Qualitative and Quantitative Differences in Herbivore-Induced

Plant Volatile Blends from Tomato Plants Infested by Either Tuta absoluta or Bemisia tabaci. *J. Chem. Ecol.* **2017**, *43* (1), 53−65.
(13) Abdollahipour, M.; Fathipour, Y.; Mollahosseini, A. How does a predator find its prey? Nesidiocoris tenuis is able to detect Tuta absoluta by HIPVs. *J. Asia-Pac. Entomol.* **2020**, *23* (4), 1272−1278.
(14) Qu, C.; Wang, R.; Che, W.-n.; Li, F.-q.; Zhao, H.-p.; Wei, Y.-y.; Luo, C.; Xue, M. Identification and tissue distribution of odorant binding protein genes in Harmonia axyridis (Coleoptera: Coccinellidae). *J. Integr. Agric.* **2021**, *20* (8), 2204−2213.
(15) Qu, C.; Yang, Z.-k.; Wang, S.; Zhao, H.-p.; Li, F.-q.; Yang, X.-l.; Luo, C. Binding Affinity Characterization of Four Antennae-Enriched Odorant-Binding Proteins From Harmonia axyridis (Coleoptera: Coccinellidae). *Frontiers in physiology* **2022**, *13*, 829766.
(16) Rondoni, G.; Roman, A.; Meslin, C.; Montagné, N.; Conti, E.; Jacquin-Joly, E. Antennal Transcriptome Analysis and Identification of Candidate Chemosensory Genes of the Harlequin Ladybird Beetle, Harmonia axyridis (Pallas) (Coleoptera: Coccinellidae). *Insects* **2021**, *12* (3), 209.
(17) Rodrigo, F.; Burgueño, A. P.; González, A.; Rossini, C. Better Together: Volatile-Mediated Intraguild Effects on the Preference of Tuta absoluta and Trialeurodes vaporariorum for Tomato Plants. *J. Chem. Ecol.* **2023**, *49*, 725−741.
(18) Yang, H.; Yang, W.; Yang, C. P.; Zhu, T. H.; Huang, Q.; Han, S.; Xiao, J. J. Electrophysiological and behavioral responses of the whitestriped longhorned beetle, Batocera lineolata, to the diurnal rhythm of host plant volatiles of holly, Viburnum awabuki. *Journal of insect science (Online)* **2013**, *13*, 1−11.
(19) Dallakyan, S.; Olson, A. J. Small-molecule library screening by docking with PyRx. *Methods in molecular biology (Clifton, N.J.)* **2015**, *1263*, 243−250.
(20) Mirdita, M.; Schütze, K.; Moriwaki, Y.; Heo, L.; Ovchinnikov, S.; Steinegger, M. ColabFold: making protein folding accessible to all. *Nat. Methods* **2022**, *19* (6), 679−682.
(21) Liu, D.; Liu, J.; Wang, H.; Liang, F.; Zhang, G. DeepUMQA-X: Comprehensive and insightful estimation of model accuracy for protein single-chain and complex. *Nucleic Acids Res.* **2025**, *53* (W1), W219−W227.
(22) Ye, B.; Tian, W.; Wang, B.; Liang, J. CASTpFold: Computed Atlas of Surface Topography of the universe of protein Folds. *Nucleic Acids Res.* **2024**, *52* (W1), W194−w199.
(23) Minh, B. Q.; Schmidt, H. A.; Chernomor, O.; Schrempf, D.; Woodhams, M. D.; von Haeseler, A.; Lanfear, R. IQ-TREE 2: New Models and Efficient Methods for Phylogenetic Inference in the Genomic Era. *Mol. Biol. Evol.* **2020**, *37* (5), 1530−1534.
(24) Kalyaanamoorthy, S.; Minh, B. Q.; Wong, T. K. F.; von Haeseler, A.; Jermiin, L. S. ModelFinder: fast model selection for accurate phylogenetic estimates. *Nat. Methods* **2017**, *14* (6), 587−589.
(25) Hoang, D. T.; Chernomor, O.; von Haeseler, A.; Minh, B. Q.; Vinh, L. S. UFBoot2: Improving the Ultrafast Bootstrap Approximation. *Mol. Biol. Evol.* **2018**, *35* (2), 518−522.
(26) Amaro, R. E.; Baudry, J.; Chodera, J.; Demir, O.·.; McCammon, J. A.; Miao, Y.; Smith, J. C. Ensemble Docking in Drug Discovery. *Biophys. J.* **2018**, *114* (10), 2271−2278.
(27) Holdgate, G. A. Kinetics, Thermodynamics, and Ligand Efficiency Metrics in Drug Discovery. In *Comprehensive Medicinal Chemistry III*; Chackalamannil, S., Rotella, D., Ward, S. E., Eds.; Elsevier: Oxford, 2017; pp 180−211.
(28) Schrödinger, M. *SchröDinger Release 2018−1*; Schrödinger, LLC: New York, NY, 2018.
(29) Shaw, S. R. a. D. E. Desmond Molecular Dynamics System. *Shaw Res. N. Y. NY* **2019**.
(30) Roos, K.; Wu, C.; Damm, W.; Reboul, M.; Stevenson, J. M.; Lu, C.; Dahlgren, M. K.; Mondal, S.; Chen, W.; Wang, L.; Abel, R.; Friesner, R. A.; Harder, E. D. OPLS3e: Extending Force Field Coverage for Drug-Like Small Molecules. *J. Chem. Theory Comput.* **2019**, *15* (3), 1863−1874.
(31) Boulaamane, Y.; Ahmad, I.; Patel, H.; Das, N.; Britel, M. R.; Maurady, A. Structural exploration of selected C6 and C7-substituted coumarin isomers as selective MAO-B inhibitors. *Journal of Biomolecular Structructure and Dynamics* **2023**, *41* (6), 2326−2340.
(32) Guo, J.; Liu, P.; Zhang, X.; An, J.; Li, Y.; Zhang, T.; Gao, Z. Characterization of the ligand-binding properties of odorant-binding protein 38 from Riptortus pedestris when interacting with soybean volatiles. *Frontiers in physiology* **2025**, *15*, 1475489.
(33) Venthur, H.; Zhou, J. J. Odorant Receptors and Odorant-Binding Proteins as Insect Pest Control Targets: A Comparative Analysis. *Frontiers in physiology* **2018**, *9*, 1163.
(34) De Backer, L.; Megido, R. C.; Fauconnier, M.-L.; Brostaux, Y.; Francis, F.; Verheggen, F. Tuta absoluta-induced plant volatiles: attractiveness towards the generalist predator Macrolophus pygmaeus. *Arthropod-Plant Interact.* **2015**, *9* (5), 465−476.
(35) Baud, O.; Yuan, S.; Veya, L.; Filipek, S.; Vogel, H.; Pick, H. Exchanging ligand-binding specificity between a pair of mouse olfactory receptor paralogs reveals odorant recognition principles. *Sci. Rep.* **2015**, *5* (1), 14948.
(36) Kenny, P. W. The nature of ligand efficiency. *J. Cheminf.* **2019**, *11* (1), 8.
(37) Xu, Q. W.; Wu, C.; Xiao, D.; Jin, Z.; Zhang, C.; Hatt, S.; Guo, X.; Wang, S. Ecological function of key volatiles in Vitex negundo infested by Aphis gossypii. *Front. Plant Sci.* **2023**, *13*, 1090559.
(38) Peñaflor, M. F.; Bento, J. M. Herbivore-induced plant volatiles to enhance biological control in agriculture. *Neotrop. Entomol.* **2013**, *42* (4), 331−343.
(39) Boncan, D. A. T.; Tsang, S. S. K.; Li, C.; Lee, I. H. T.; Lam, H. M.; Chan, T. F.; Hui, J. H. L. Terpenes and Terpenoids in Plants: Interactions with Environment and Insects. *Int. J. Mol. Sci.* **2020**, *21* (19), 7382.
(40) Chiu, C. C.; Keeling, C. I.; Bohlmann, J. Toxicity of Pine Monoterpenes to Mountain Pine Beetle. *Sci. Rep.* **2017**, *7* (1), 8858.
(41) Binyameen, M.; Ali, Q.; Roy, A.; Schlyter, F. Plant Volatiles and Their Role in Insect Olfaction. In *Plant-Pest Interactions: From Molecular Mechanisms to Chemical Ecology: Chemical Ecology*; Singh, I. K., Singh, A., Eds.; Springer Singapore: Singapore, 2021; pp 127−156.
(42) Kaplan, I. Attracting carnivorous arthropods with plant volatiles: The future of biocontrol or playing with fire? *Biol. Control* **2012**, *60* (2), 77−89.
(43) Gregg, P. C.; Del Socorro, A. P.; Binns, M. R. Non-Target Impacts of an Attract-and-Kill Formulation Based on Plant Volatiles: Responses of some Generalist Predators. *J. Chem. Ecol.* **2016**, *42* (7), 676−688.
(44) Chen, T.; Chen, L.; Wang, J.; Cheng, J.; Yi, S.; Hafeez, M.; Zhou, S.; Li, Y.; Li, X.; Lu, Y. Development of attractants and repellents for Tuta absoluta based on plant volatiles from tomato and eggplant. *Frontiers in Sustainable Food Systems* **2023**, *7*, 1155317.

https://doi.org/10.1021/acs.jafc.6c01340
J. Agric. Food Chem. XXXX, XXX, XXX−XXX